RARE GAS FISSION YIELDS

OF

Am^{241} AND Am^{242}

RARE GAS FISSION YIELDS OF Am^{241} AND Am^{242}

By

JAMES FRANCIS PLEVA, B. E. Sc.

A Thesis

Submitted to the Faculty of Graduate Studies

in Partial Fulfilment of the Requirements

for the Degree

Doctor of Philosophy

McMaster University

May 1967

DOCTOR OF PHILOSOPHY (1967) McMASTER UNIVERSITY
(Physics) Hamilton, Ontario.

TITLE: Rare Gas Fission Yields of Am^{241} and Am^{242}

AUTHOR: James Francis Pleva, B. E. Sc. (University of Western Ontario).

SUPERVISOR: Professor H. G. Thode

NUMBER OF PAGES: viii, 87

SCOPE AND CONTENTS:

The yields of xenon and krypton from the neutron-induced fission of Am^{241} and Am^{242} have been measured with a mass spectrometer. This was accomplished by irradiating samples of Am^{241} for different lengths of time so that the effect of the growth of highly fissionable Am^{242} could be determined.

These studies reveal that both the degree of fine structure in the mass yield curve and the fission-product charge distribution are dependent on the energy of the incident neutrons. This has not been previously observed for any fissioning nuclide. These studies also reveal effects of the 50-neutron shell and of the neutron-proton ratio of the fissioning nuclide on the mass yield curve.

ACKNOWLEDGMENTS

I wish to express my sincere appreciation to Dr. H. G. Thode for his inspiration and guidance throughout the course of this investigation. I would also like to thank Dr. W. B. Clarke and Dr. R. H. Tomlinson for many helpful discussions.

Generous financial assistance was provided by the National Research Council, Government of Ontario, and McMaster University.

TABLE OF CONTENTS

LIST OF TABLES

LIST OF ILLUSTRATIONS

INTRODUCTION

The discovery of nuclear fission in 1939 by Hahn and Strassmann (1) heralded the direct exploitation of nuclear energy on a large economic scale. However, the exact nature of the fission process itself is still not completely understood and much investigation, both theoretical and experimental, is in progress in the hope of gaining a clearer insight. The experimental work described in the thesis forms a part of this investigation.

Since the discovery of fission, much progress has been made in determining some of the basic features of the fission process. As early as February 1939, Meitner and Frisch (2), who invented the phrase "nuclear fission", likened the behaviour of a fissioning nucleus to that of a liquid drop. The surface tension energy of this nuclear drop is provided by the short-range nuclear forces and the deforming energy is provided by the long-range repulsive Coulomb forces. In the case of slow-neutron induced fission of uranium, which was the first type of fission studied, additional deforming energy is provided by the excitation resulting from neutron capture. If the deforming energy is sufficient to overcome the surface tension energy barrier, the nucleus will divide into two parts attaining a total kinetic energy of about 200 Mev.

On the basis of the liquid drop model, Bohr and Wheeler (3) calculated that U^{235}, and not the more abundant U^{238}, is responsible for the slow neutron fission of uranium. Shortly thereafter, Nier, Booth, Dunning and Grosse (4) tested this prediction by separating U^{235} and U^{238} in an electromagnetic separator and irradiating each isotope with both slow and fast neutrons. Measurements of the relative

fission rates verified the prediction and also showed that U^{238} is mainly responsible for the fast neutron fission of natural uranium.

It is now known that many heavy nuclides can be made to undergo fission and that fission can be induced by a great variety of particles or can occur spontaneously. Also, a number of models of the fission process have been devised. Many of these are modifications of the liquid drop model.

MEASUREMENT OF FISSION YIELDS

Mass Distribution

When a nucleus undergoes fission, the mass can be distributed in many ways among the outgoing particles. Equation (1) represents a typical fission event for U^{235}.

$$ {}_{92}U^{235} + {}_{0}n^{1} \longrightarrow {}_{Z_1}X_1^{A_1} + {}_{Z_2}X_2^{A_2} + \nu({}_{0}n^{1}) + Q \quad . \; . \; . \; (1) $$

where X is a fission product

ν is the number of neutrons emitted

Q is the energy released as gamma rays and kinetic energy.

A_1 and A_2 can have any of a large assortment of values provided that $A_1 + A_2 + \nu = 236$. The yield of a particular mass chain A is defined as the number of fission product atoms of mass A divided by the total number of fissions. Because of the high neutron-to-proton ratio in the uranium mass region, the fission products are usually neutron rich and in most chains they beta-decay to a single stable isotope. Figure 1 shows a typical decay chain ending at Xe^{131}.

The average number of neutrons emitted per fission is about 2.5 for U^{235} making possible a chain reaction. Over 99% of these

FIGURE 1 TYPICAL MASS CHAIN

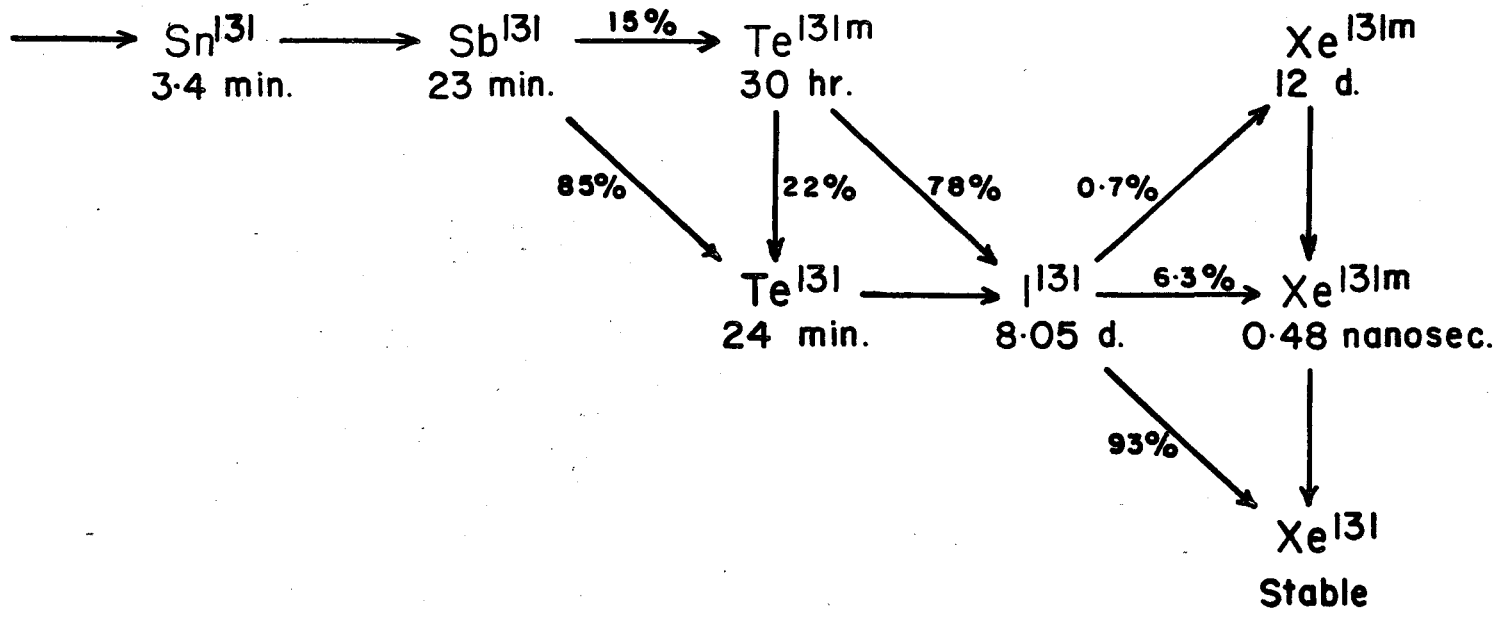

neutrons are emitted from the fission fragments immediately after fission when the fragments have reached about 90% of their final velocity. These are therefore referred to as prompt neutrons. Delayed neutrons are emitted from some fragments as much as one minute after the corresponding fission events and it is through this phenomenon that nuclear chain reactions can be controlled as in a nuclear reactor. The effect of prompt and delayed neutron emission on fission yields will be discussed shortly.

The first yield measurements were made using radiochemical techniques. The usual procedure was to measure the activity of a relatively long-lived isotope near the end of a decay chain. For example, I^{131} was used for the 131 mass chain. The accuracy of this type of measurement is of the order of 10%. The results for the thermal neutron fission of U^{235} and Pu^{239} and for the fast fission of U^{238} (5) showed a strong preference for asymmetric fission as can be seen in Figure 2. This was not expected from the liquid drop model. Also, the light mass hump of the yield curve is shifted to the right if the mass of the fissioning nucleus is greater. At the same time, there is no shift in the heavy mass curve. These results indicate a general preference in the fission act for the heavy fragment to contain closed shells of 82 neutrons and 50 protons.

More accurate yield measurements can be made using mass spectrometric techniques. In this case, the amount of a stable end product is usually measured, e.g. Xe^{131}. The precision of these measurements is of the order of 1%. In 1947, Thode and Graham (6) analyzed the fission product xenon and krypton produced in the thermal neutron fission of U^{235}. This gave the 83, 84, 85, 86, 131, 132, 134 and 136 mass chain yields. All yields except the 84 and 134 yields lay on the smooth, radiochemically determined curve. The exceptional

FIGURE 2 MASS YIELD CURVES FOR U^{235}, Pu^{239}, AND U^{238} FROM EARLY RADIOCHEMICAL INVESTIGATIONS

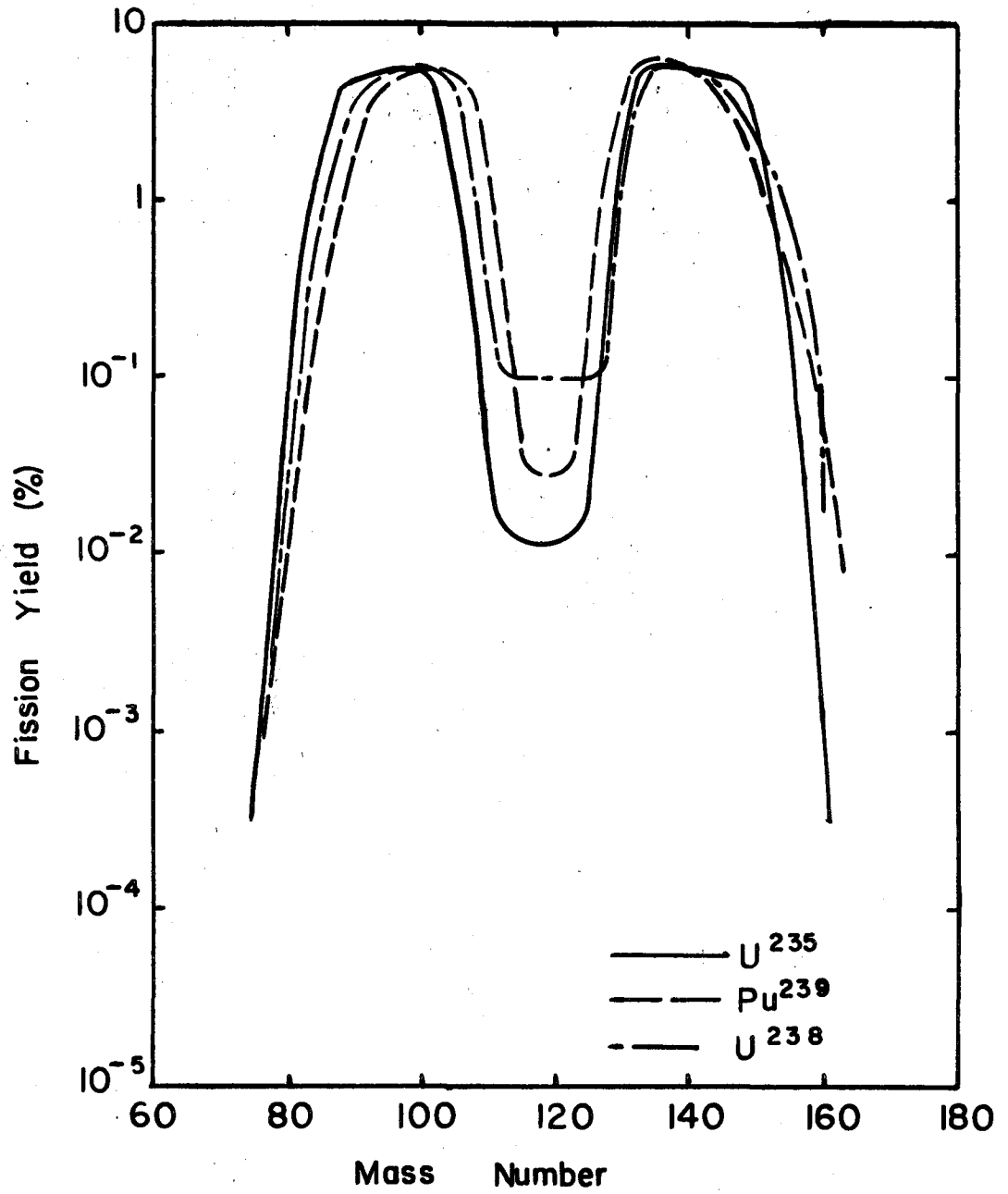

yields were 35% high proving the existence of fine structure in the yield curve. Later, in 1950, the 133 yield was found to be 25% high (7). A complete yield curve showing that fine structure exists at many different masses was derived by Petruska et al. (8) and revised by Farrar et al. (9, 10). The latter curve is shown in Figure 3.

The yield curves for other fissile nuclides show varying degrees of fine structure. For the thermal neutron fission of Pu^{239} (11) and Pu^{241} (12) there exists a very prominent peak at mass 134. Spontaneous (13) and fast neutron (14) fission of U^{238} give an excessive yield at mass 132. The heavy mass hump for the thermal neutron fission of Th^{229} (15) shows prominent wings at masses 134 and 144. Thermal neutron fission of U^{233} shows only slight fine structure (16).

The above examples of fine structure have been measured mass spectrometrically. Radiochemical yield measurements on the spontaneous fission of Cm^{242} (17), Cf^{252} (18) and Pu^{240} (19), the 15 Mev deuteron-induced fission (20) of U^{235} and U^{238}, and the photo-induced fission of U^{238} (21, 22) also show fine structure.

A number of explanations for the existence of fine structure have been put forward. Glendenin (23) proposed that any nuclide with 83 neutrons tends to "boil off" the 83rd neutron so as to obtain the stable 82 neutron configuration. Pappas (24) extended this hypothesis to cover 85, 87 and 89 neutron configurations. However, if this were the only mechanism which affected an otherwise smooth yield curve, there would be depressions adjacent to the peaks which are deep enough to compensate for the heights of the peaks. The lack of sufficiently deep depressions and also the presence of a peak at mass 100 (for thermal neutron fission of U^{235} (25)), which is complementary to the peak at 134, gave reason to believe that structural preference in the primary fission act also plays a significant role (26).

FIGURE 3 MASS YIELD CURVE OF U^{235} FROM RECENT MASS SPECTROMETRIC MEASUREMENTS

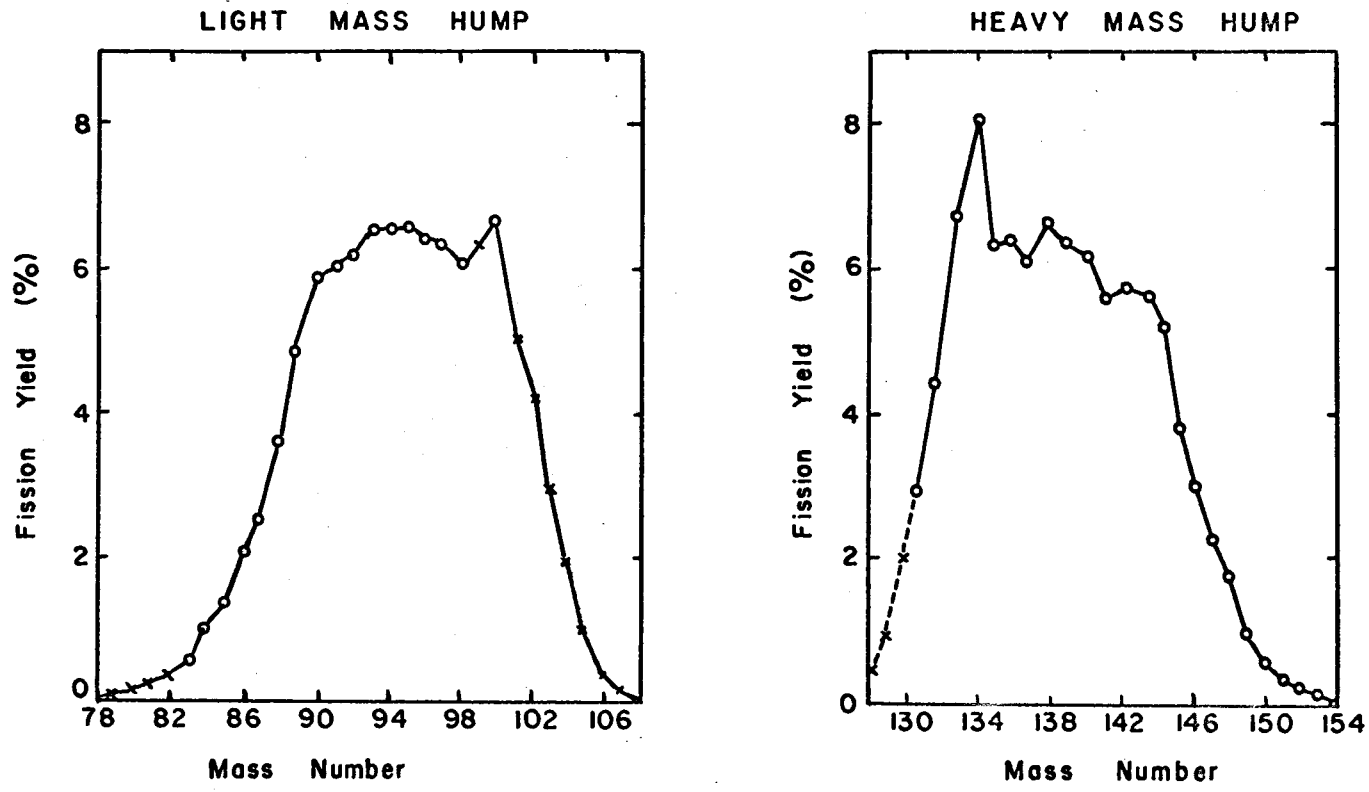

The fact that fine structure occurs at lower mass numbers for U^{238} than for U^{235} verifies the importance of the 82 neutron shell. This is because U^{238} has a higher neutron-to-proton ratio than U^{235} and therefore the fission fragments from U^{238} will likely have higher neutron-to-proton ratios. Therefore, the fragments from U^{238} containing 82 or 83 neutrons will be lighter than those from U^{235} containing the same number of neutrons.

Delayed neutron emission produces a slight amount of fine structure. For example, I^{137} has a slight effect on the top of the heavy mass hump and Br^{87} an even smaller effect on the lower slope of the light mass hump.

Neutron absorption by fission products with high capture cross sections also produces fine structure. However, it is usual to correct for this effect rather than consider it as a true fine structure. Xe^{135}, Sm^{149}, and Sm^{151} are the only fission products that have large enough cross sections to have an appreciable effect. By using short irradiation times and low fluxes, the effect can be reduced.

The most recent explanation of fine structure has been put forward by Farrar and Tomlinson (27). It is now known that the number of neutrons emitted per fragment increases as one progresses from the light mass side to the heavy mass side of each hump in the yield curve (28, 29). Also, a prompt yield curve (i.e., for yields of fragments before neutron emission) has been measured for U^{235} by Milton and Fraser (30) using time-of-flight techniques. Farrar and Tomlinson showed that slight fluctuations in the neutron emission probability versus fission fragment mass number curve would generate large amounts of fine structure even if the prompt yield curve were perfectly smooth. By correlating their own fission yield curve (for fragments after neutron emission) with the prompt yield curve, they were able to

generate a neutron emission probability curve similar to that measured directly by Apalin et al. (29) for U^{235}.

Charge Distribution

Up to this point, we have been concerned only with the total yield of a given mass chain. An independent yield, on the other hand, is the fraction of the number of fissions which give fission products of a given mass number A and a given atomic number Z before beta decay has a chance to occur. It is generally accepted that an independent yield refers to fission products as they exist immediately after prompt neutron emission. Therefore, the sum of the independent yields for a given mass number is equal to the total yield for that mass number except in the few cases where delayed neutron emission produces chain branching.

When one speaks of charge distribution in nuclear fission, one is usually referring to the distribution of independent yields within a given mass chain. It is now believed that the shape of a typical distribution curve is that shown in Figure 4. Because Z_p, the most probable charge, is so far removed from Z_A, the charge of the most stable nuclide of mass A, the primary fission products beta-decay very rapidly. This makes the measurement of independent yields very difficult. However, in the mass chain shown in Figure 5 there is a stable nuclide at Z = 52 and another at Z = 54. As a result, no primary fission products of $Z < 53$ can beta-decay to Xe^{130}. Also, the independent yield of I^{130} will be much greater than that of Xe^{130} because of the steepness of the charge distribution curve in that region. Therefore, by measuring the amount of Xe^{130} produced after I^{130} has entirely decayed, one can determine the independent yield of I^{130}. I^{130} is referred to as a shielded nuclide.

FIGURE 4 CHARGE DISTRIBUTION IN FISSION

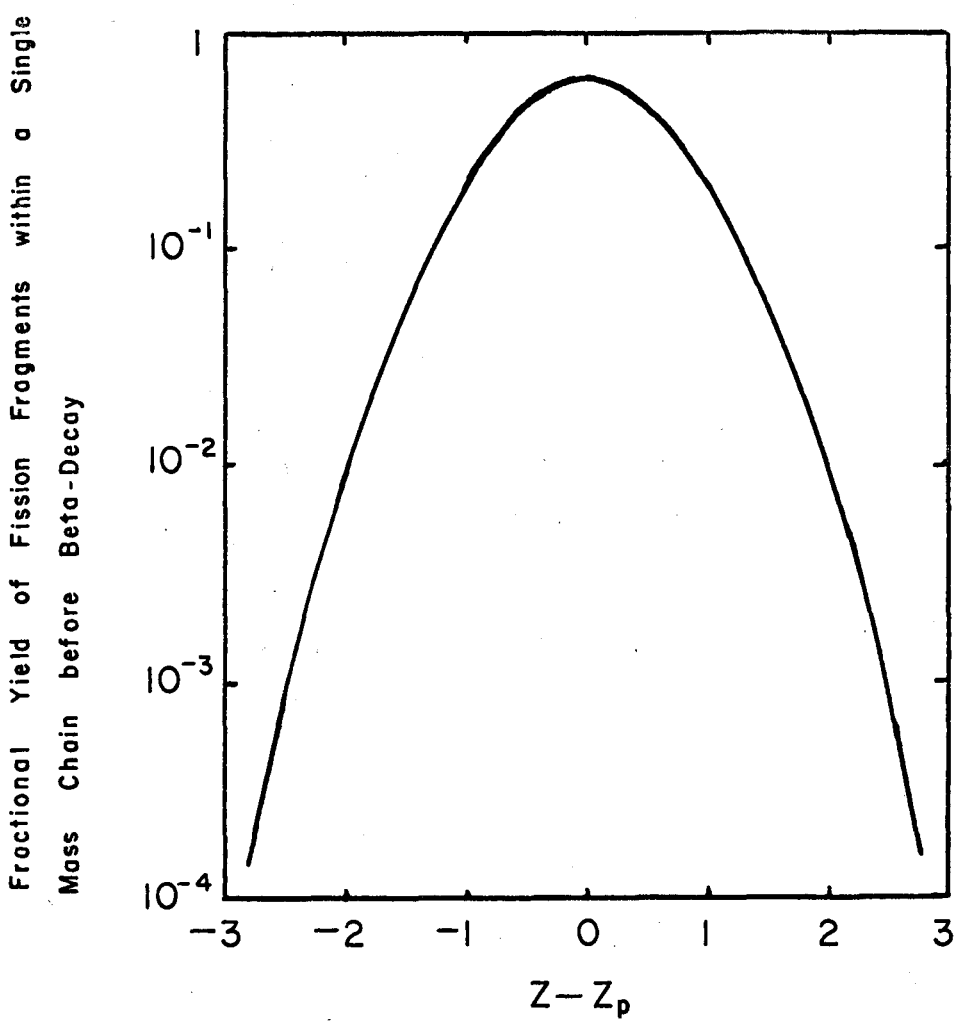

where Z = charge of fission fragment

and Z_p = most probable charge

FIGURE 5 MASS CHAIN WITH SHIELDED NUCLIDE

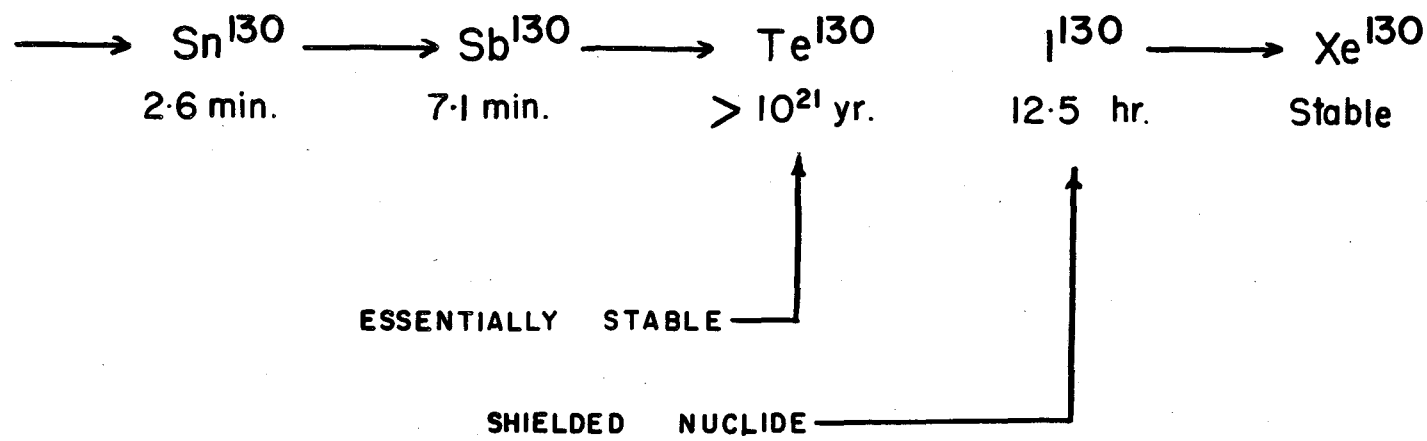

The measurement of shielded nuclides by radiochemical and mass spectrometric techniques has resulted in a number of postulates concerning both the shape of the distribution curve and the value of Z_p. Recently, Wahl and co-workers (31) have derived radiochemical methods for measuring independent yields of several unshielded nuclides on the same mass chain. The results indicate that none of the postulates previously proposed is entirely correct. Nevertheless, it is instructive to review two of these postulates.

The postulate of equal charge displacement was first suggested by Glendenin, Coryell, and Edwards (32). It states that the most probable charge, Z_p, is displaced from the most stable charge, Z_A, by the same amount for each fragment, i.e.

$$(Z_p - Z_A)_{light} = (Z_p - Z_A)_{heavy}$$

The Z_A values were originally taken from the Bohr-Wheeler stability curve, but a later revision by Pappas (33) used the Coryell, Brightsen, Pappas stability curve which takes into account the extra stability of the closed shell configurations. The shape of the charge distribution curve was assumed to be a Gaussian in the middle and a rapidly diminishing logarithmic function on the extremities. Also, it was assumed to be the same at all masses.

In 1956, Kennett and Thode (34) suggested that Z_p might be determined by the requirement that the energy released in the fission process be a maximum. For example, in the thermal neutron fission of U^{235}, the quantity

$$\left[M({}_{92}U^{235}) + M({}_{0}n^{1}) - M({}_{Z_1}X^{A_1}) - M({}_{Z_2}X^{A_2}) - \nu M({}_{0}n^{1})\right]$$

should be a maximum. The Z_p values calculated in this way are plotted in Figure 6 along with those calculated according to the postu-

FIGURE 6 RELATIONSHIP BETWEEN MOST PROBABLE CHARGE AND MASS NUMBER OF FISSION FRAGMENT

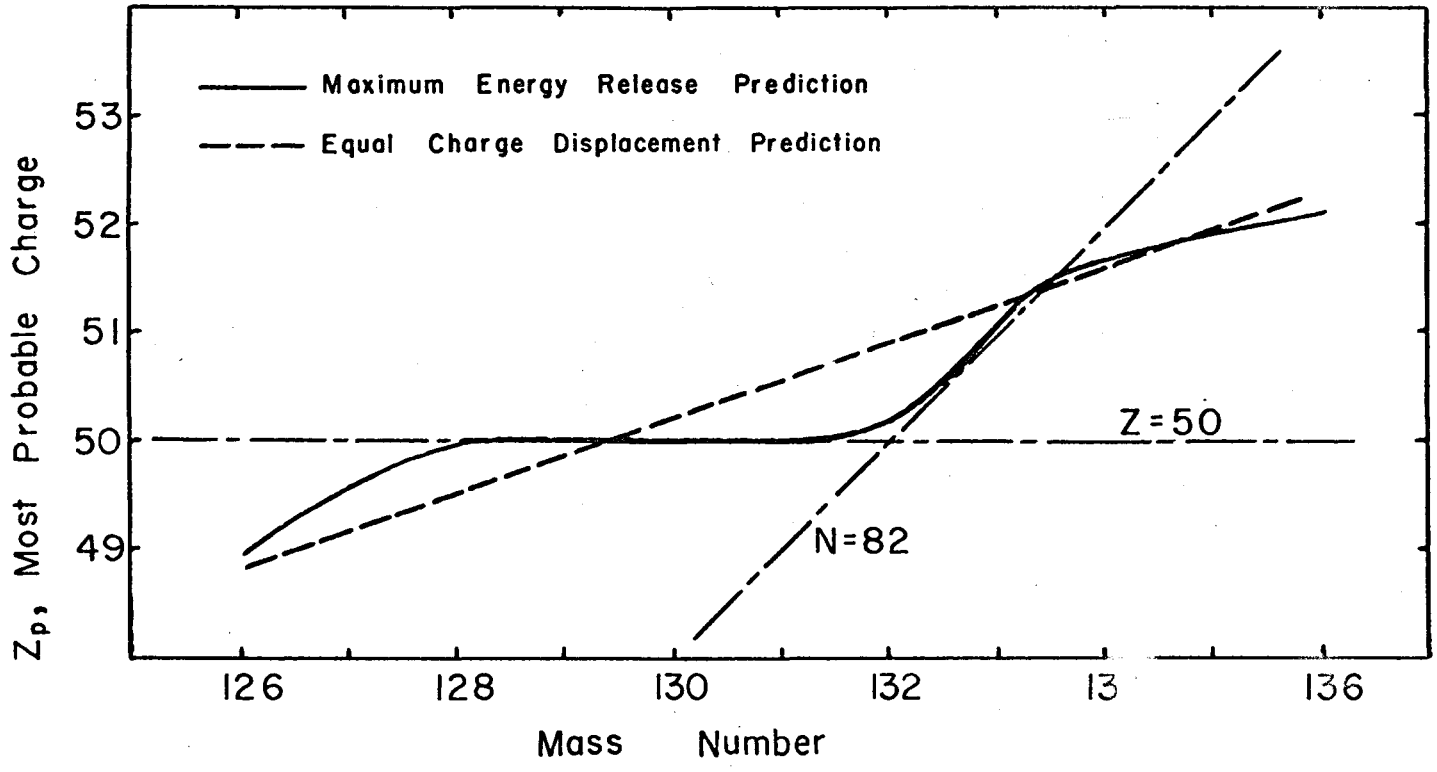

late of equal charge displacement. As can be seen, the postulate of maximum energy release favours the formation of fission products with closed shells more than does the postulate of equal charge displacement.

Experiments on U^{235} which were performed in connection with the present project but which are not described herein show that the value of Z_p does indeed deviate from the equal charge displacement prediction in the direction of the closed shells for mass chains 80, 82, 128, and 130, but not to the extent predicted by maximum energy release.

MODELS OF THE FISSION PROCESS

The failure of the liquid drop model to predict the observed asymmetry in the fission yield curve has resulted in the development of other models. The essential characteristic of these models is the incorporation of closed shell effects. These are introduced either directly or indirectly. The shells which play the most significant role in nuclear fission are the 82 neutron and 50 proton shells for the heavy fragments and the 50 neutron shell for the light fragments.

Fong (35) has developed a statistical mechanical model whereby the nucleons in the fissioning nucleus are assumed to come to statistical equilibrium just prior to the fission act according to the level densities of the fission fragments to be formed. Since the level densities depend on the excitation energies of the fragments, it is necessary to know the ground state masses of the fragments. Fong used his own semiempirical mass formula which takes into account shell effects. Among other successes, his model predicts very well the observed mass yield and charge distribution patterns for the thermal neutron fission of U^{235}. It is less successful with the thermal neutron fission of Pu^{239}. Also, contrary to experimental results (36), it predicts a

large variation in the total number of neutrons emitted as a function of mass ratio of the fission fragments.

A model recently developed by Brunner and Paul (37) considers the effect of the deformation of the fission fragments on the potential barrier through which the fragments must pass. Fragments which contain closed shell configurations deform much less readily than those which do not. Calculations (38, 39) based on this model reproduce the observed fission yield curves for the thermal neutron fission of U^{235} and U^{233} but fail for the thermal neutron fission of Pu^{239} and Th^{229} and for the independent yield curves determined by Wahl (31).

Reference has already been made to experiments which reveal the number of prompt neutrons emitted by fragments of various masses. The results obtained by Whetstone (28) on the spontaneous fission of Cf^{252} (see Figure 7) appear to be typical of many fissioning nuclei (29, 40). Whetstone interpreted his results with a highly qualitative but intuitively satisfying model of the fission process. According to the liquid drop model, the nucleus assumes a dumb-bell shape just prior to fission. Whetstone modified this by postulating that one end is larger than the other and that Coulomb repulsion of the protons makes the neck rich in neutrons. The probability that the neck will break at a given point is greater where the neck is thinner. Therefore, asymmetric fission which corresponds to a break in the middle of the neck is highly probable. Symmetric fission which corresponds to a break at the far left end of the neck is very unlikely to occur. Also, the fragment which carries away the larger part of the neck will emit more prompt neutrons. It can be seen that this is in accordance with curves in Figure 7.

Whetstone did not say definitely that shell structure was the cause of the ends of the dumb-bell being of different size. Mathews and Tomlinson (41), however, proposed a very similar model as shown

FIGURE 7 WHETSTONE MODEL OF FISSION

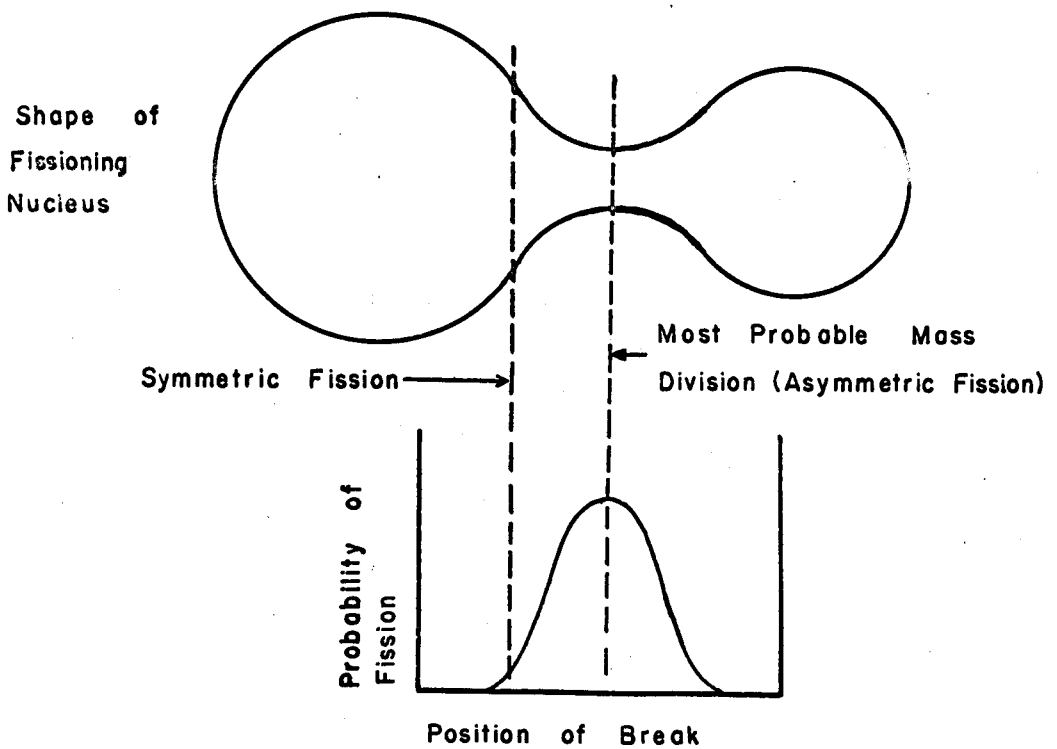

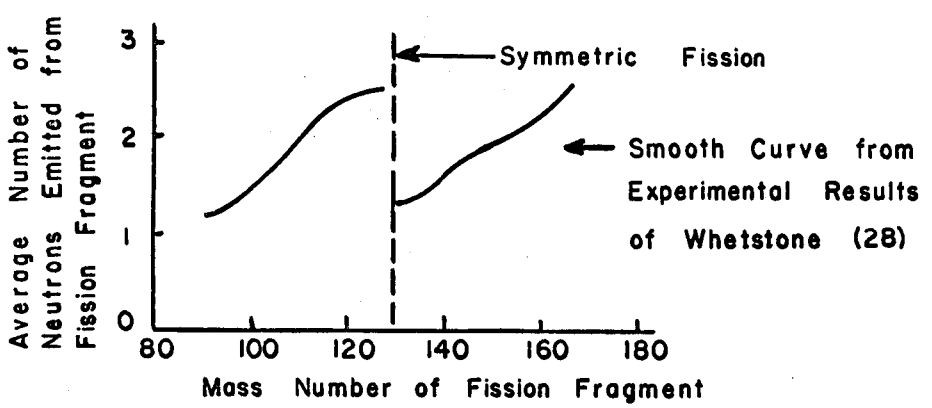

in Figure 8 in which the heavy end contains the 82 neutron and 50 proton shells and the light end contains the 50 neutron shell. The indentations next to the spheres were proposed to account for the general tendency of fission yield humps to contain wings on the sides.

In the foregoing discussion of models, emphasis has been given to success or failure in predicting fission yields. Other measured variables, such as probability of spontaneous fission and variation of kinetic energy release with the mass ratio of fission fragments, have also been predicted with varying degrees of success. Nevertheless, no single model has been able to account for all the observed fission phenomena.

AMERICIUM FISSION YIELDS

Americium is an artificially produced element of atomic number 95. It was first identified in 1944 by Seaborg, James, Morgan and Ghiorso (42, 43) and was produced by the extensive irradiation of Pu^{239} according to the following set of reactions:

$$Pu^{239}(n,\gamma)\,Pu^{240}(n,\gamma)\,Pu^{241} \xrightarrow[13.2\,y]{\beta^-} Am^{241}.$$

This is still the method commonly used for producing Am^{241}.

The yields from the thermal neutron fission of Am^{241} have been measured radiochemically for a number of mass chains (44, 45). The work described in this thesis represents the first mass spectrometric measurements of americium fission yields. There are a number of reasons why this has not been attempted before. They can be summarized as follows:

(a) small fission cross-section of Am^{241},

(b) growth of highly fissionable Am^{242} during irradiation,

(c) hazard involved in handling alpha-emitters of high specific activity.

FIGURE 8 MATHEWS–TOMLINSON MODEL OF FISSION

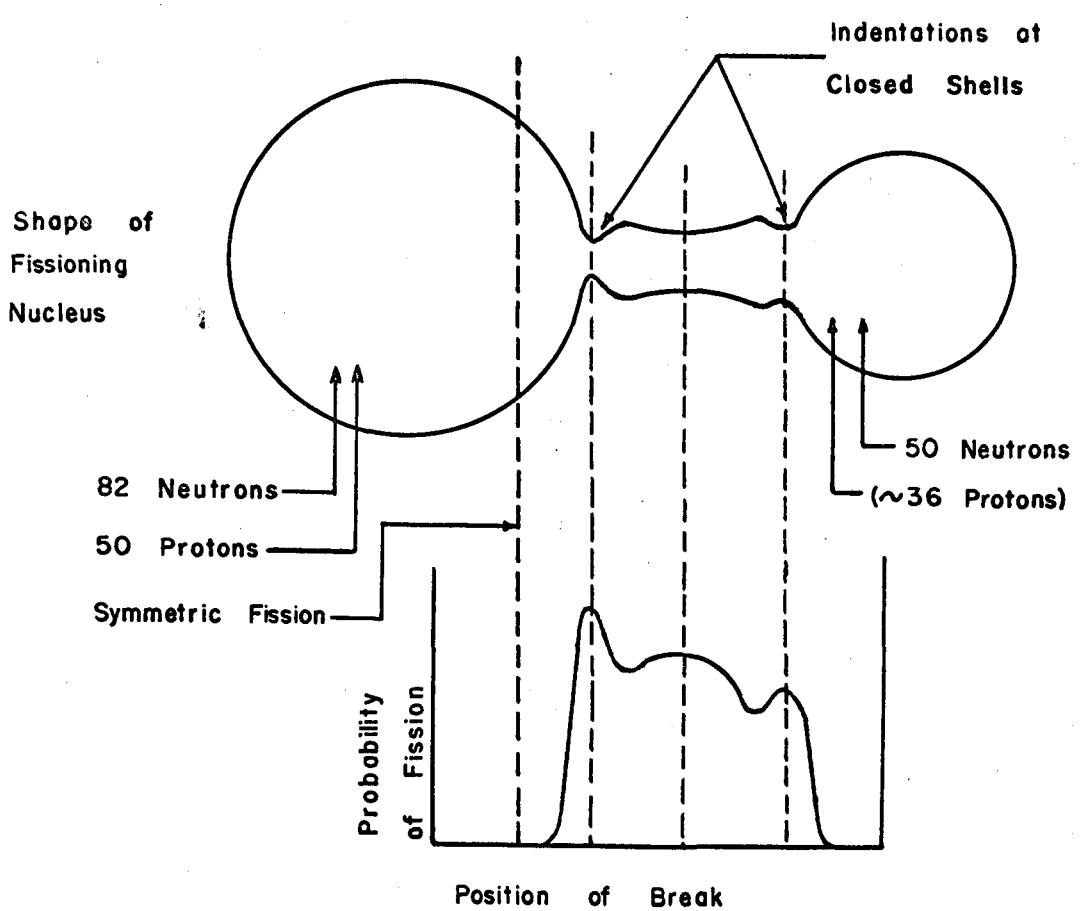

These will now be discussed in detail.

The thermal neutron fission cross-section of Am^{241} is 3.13 ± 0.15 barns. This is quite small compared to typical fissionable nuclides such as U^{235}, U^{233}, and Pu^{239} whose fission cross-sections lie between 500 and 800 barns. The measurement of isotopic ratios in a mass spectrometer is easier and more accurate for larger samples. Therefore, in order to measure the fission yields of a nuclide with a low fission cross-section, one would be tempted to use long irradiation times, high neutron fluxes, and large amounts of target material.

However, the growth of highly fissionable Am^{242} during irradiation necessitates the use of low fluxes and/or short irradiation times so that most of the fission products will be the result of Am^{241} fission and not Am^{242} fission. The cross-sections leading to Am^{242} fission are shown below.

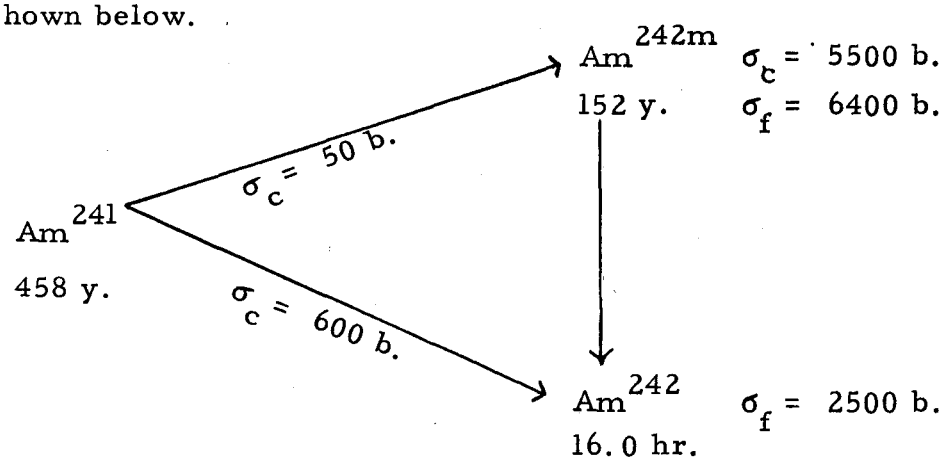

To illustrate the magnitude of the effect, an irradiation with a flux of 10^{13} neutrons per cm^2-sec. for 10 hours will result in roughly 10% of the fissions being those of Am^{242} (and Am^{242m}).

The one remaining means of offsetting the effect of a low fission cross-section is the use of large amounts of Am^{241}. However, this presents a health hazard. The half-life of Am^{241} is 458 years which means that its specific activity is nearly four times that of Ra^{226},

Radium and most other heavy elements, including americium, tend to remain locked in the body if breathed or ingested. The maximum tolerable amount of an alpha-emitter that can be accumulated over a lifetime is 0.04 μ curies. This amount is referred to as one body burden and for Am^{241} weighs only 0.01 μg. Therefore, if one is to use large quantities, special handling procedures must be developed and consistently followed.

The measurement of xenon and krypton yields with a mass spectrometer gives information which cannot be obtained radiochemically. One of the most interesting regions of a fission yield curve is from mass 131 to mass 136 where closed shell effects are most pronounced. The most accurate radiochemical measurements in this region so far performed on the thermal neutron fission of Am^{241} (45) have an accuracy of 5%. Relative yields in this region which are accurate to 0.5% would not only be useful in themselves, but would reveal subtle changes in the fine structure resulting from different irradiation conditions. For example, the irradiation of a number of samples for different lengths of time would show progressive changes in the yield pattern due to the growth of Am^{242}. Also, small changes in fine structure resulting from irradiation with neutrons of different energy may be apparent.

In the krypton region, no previous yield measurements of any kind have been made. These yields should lie on the lower slope of the light mass hump. One would expect large changes in the xenon to krypton yield ratio as the number of Am^{242} fissions increases with respect to that for Am^{241}. This is because the light mass hump should shift to the right.

With these possibilities in mind, mass spectrometric measurements were made of the yields of xenon and krypton from the neutron-

induced fission of Am^{241} and Am^{242} under various irradiation conditions.

EXPERIMENTAL

PREPARATION OF Am^{241} FOR IRRADIATION

Americium-241 is an alpha emitter of high specific activity. However, in order to obtain sufficient quantities of fission product xenon and krypton for mass spectrometric analysis, it is necessary to irradiate milligram quantities of americium. Since one milligram of Am^{241} contains 10^5 body burdens, special precautions are required in its handling.

The americium used in this series of experiments was obtained from Oak Ridge National Laboratories. The glass vial containing 20 mg of black oxide powder, AmO_2, was removed from its lead shipping container in a glove box and carefully opened. Six drops of 8M HCl were added and within 24 hours all of the AmO_2 had dissolved to form a bright yellow solution. This is the characteristic colour of Am^{+3} ion in high concentration (46).

Repurification of Am^{241}

Am^{241} is produced by the β-decay of Pu^{241} which has a high fission cross-section of 1.0×10^3 barns for pile neutrons. Therefore, to measure the fission yields of Am^{241}, it is essential that all Pu^{241} be completely removed from the Am^{241}. Although the purity specifications which accompanied the shipment of Am^{241} did not mention the presence of a significant amount of Pu^{241}, it was considered a wise precaution to repurify the sample and, by so doing, set an upper limit on the amount of Pu^{241} present.

The americium was repurified by means of the following process

(47). The amount to be repurified at any one time (usually about 6 mg) is converted to a few drops of solution containing 8M HCl and 0.1M HNO_3. After sitting for at least one hour, this solution is then passed through an ion exchange column 5 cm long and 2 mm in diameter, containing Dowex 1 x10 200-400 mesh anion exchange resin. Because americium remains in the Am^{+3} state in concentrated HCl but plutonium forms an anionic chloride complex, the americium passes through the column whereas the plutonium remains on the resin. (The presence of 0.1M HNO_3 ensures the complete oxidation of Pu^{+3} to Pu^{+4} or Pu^{+6}. Pu^{+3} does not form an anionic chloride complex whereas Pu^{+4} and Pu^{+6} do.) The americium is washed through with more 8M HCl - 0.1M HNO_3 and collected in a separate vial. Then distilled water is added to the column causing the plutonium chloride complex to dissociate, thereby allowing the plutonium to pass through the column.

It should be noted that it is necessary to prepare the ion exchange column by passing 8M HCl - 0.1M HNO_3 through it for at least three hours prior to introducing the americium to the column. It is also wise to prepare the acid mixture within 12 hours of use because of the tendency of the HNO_3 to decompose in concentrated HCl.

Before repurifying the large amounts of americium, as described above, the repurification process was tested using an artifically prepared mixture of Pu^{241} and Am^{241}. Individual drops were collected from the bottom of the column on stainless steel planchets (2 drops per planchet), evaporated to dryness, and placed in a proportional counter which was set up to distinguish between 5 Mev α-particles from Am^{241} and 20 Kev β-particles from Pu^{241}.

The counting rates are shown in Figure 9. Planchet no. 1 was placed under the column immediately after depositing the Am-Pu mixture. The counting rate for planchet no. 1 indicates that the Am^{241}

FIGURE 9 TESTING OF REPURIFICATION PROCESS

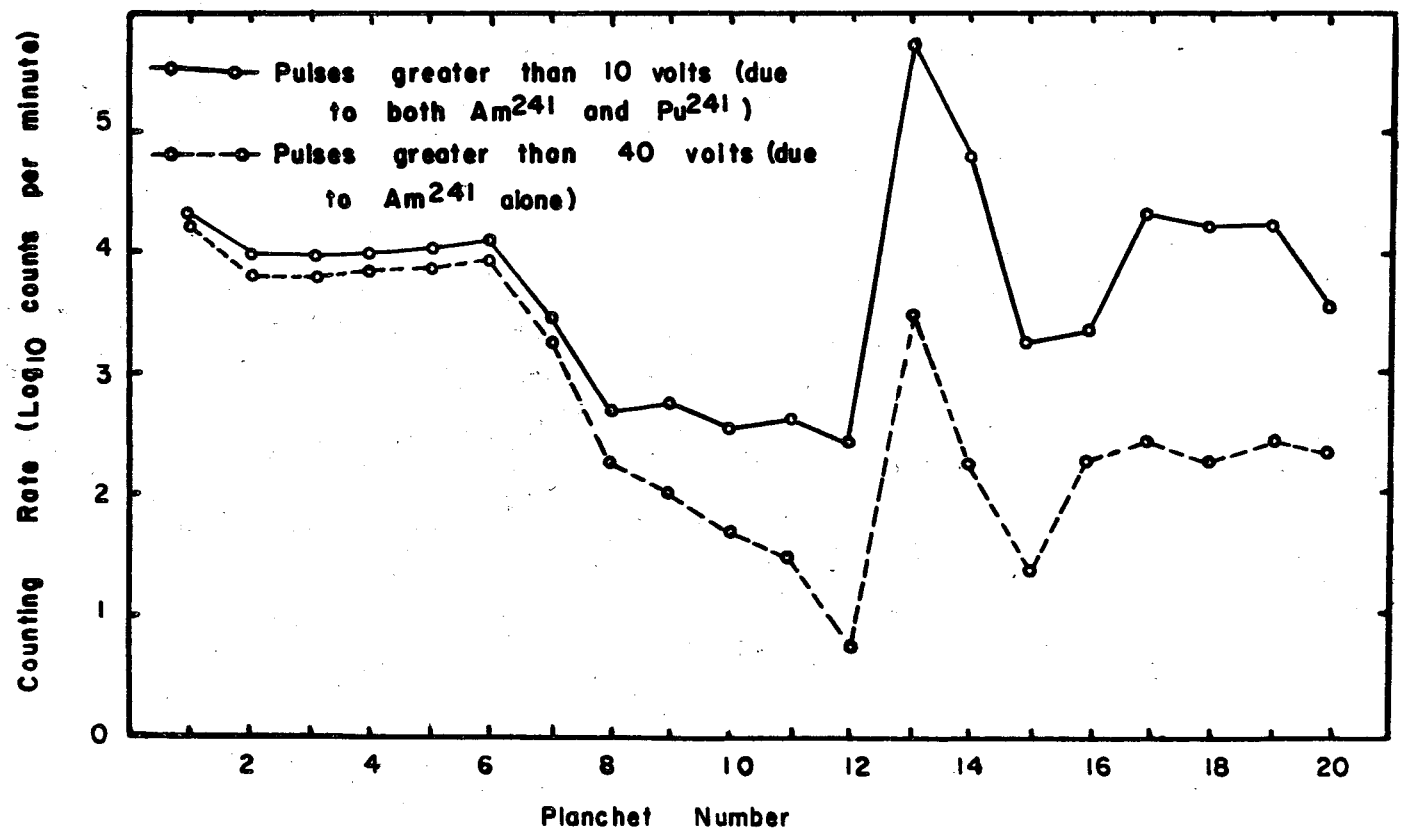

diffuses freely through the column. 8M HCl - 0.1M HNO_3 was added to the column periodically to wash the Am^{241} through. When planchet no. 11 was placed under the column, distilled water was added. The boundary between the acid and the distilled water was clearly visible in the column and did not reach the bottom until planchet no. 13 was under the column. This is reflected in the observed counting rates which indicate that most of the Pu^{241} came through with the first drops of distilled water. More distilled water was added to the column periodically to wash out the remaining plutonium.

Analysis of the counting rates shown in Figure 9 indicates that a maximum of 2.9% of the Pu^{241} could have passed through the column before planchet no. 13 was placed under the column. Because ion exchange columns are equally retentive at any concentration below saturation, this purification process therefore removes a minimum of 97.1% of the Pu^{241} from a mixture of Am^{241} and Pu^{241}.

In order to determine the amount of Pu^{241} in the 20 mg of Am^{241} sent from Oak Ridge National Laboratories, 1 mg of it was repurified using a fresh ion exchange column, and the Pu^{241} retained on the column was completely washed off with a large quantity of distilled water and stored for one year. Then one drop of this was evaporated to dryness on a stainless steel planchet and the Am^{241} which had grown in from β-decay of Pu^{241} was counted with a portable alpha monitor. A small, known fraction of the original Am^{241} was placed on another planchet and similarly counted. The two count rates, which were within a factor of 5 of each other, were within the optimum range of the instrument, and thereby allowed an accurate determination of the upper limit of the amount of Pu^{241} present. This method is superior to counting the Pu^{241} directly in a proportional counter because there is no need to correct for the relative counting efficiency of 20 Kev β's

with respect to 5 Mev α's. The upper limit was calculated to be 17 μg of Pu^{241} per mg of Am^{241}. However, the true Pu^{241} content is undoubtedly much lower than this, the excessively high counting rate likely being the result of traces of the large amount (1 mg) of Am^{241} that was repurified. Nevertheless, to be on the safe side, it was decided to accept 17 μg Pu^{241} per mg Am^{241} as being the upper limit.

Having now determined the maximum possible Pu^{241} contamination and the effectiveness of the repurification process, it can be shown that two successive repurifications will reduce the Pu^{241} content to the extent that less than 0.5% of the number of fissions will be of Pu^{241}. Therefore, the Am^{241} used in the following experiments was repurified twice using a fresh column each time.

Evaporation and Sealing-off Procedures

After repurification, the americium solution was evaporated to dryness on a Teflon dish and redissolved in 1.5M HNO_3 three times in order to remove as much HCl as possible. The concentration of Am^{241} was adjusted so that one drop would contain approximately 0.5 mg of Am^{241}. If the sample being prepared was to be irradiated for a long period of time, one drop of this solution was placed on a piece of aluminium foil 14 mm square by 0.001 inches thick. For shorter irradiations, larger amounts (up to 1.5 mg) of Am^{241} were used, although it was found that 0.5 mg was the largest amount that could be handled conveniently. The americium solution was evaporated to as low a volume as possible, and, with the heat lamp still on, the aluminium foil was carefully folded with a pair of tweezers. The nitrate of americium appears to be extremely hygroscopic and therefore, at higher temperatures, the folding operation is much less likely to cause the americium solution to be squeezed past the edges of the foil.

It should be mentioned at this point that all operations so far described involving milligram quantities of americium were done in a glove box, and most of the instruments (polyethylene droppers, tweezers, etc.) were sealed and discarded immediately after use. However, as it was necessary to seal off the sample in an evacuated quartz break-seal capsule for irradiation, subsequent operations were performed outside the glove box.

The sealing-off procedure, which is performed using the system shown in Figure 10, was devised so that it would never be necessary to glassblow in the presence of americium. The steps of operation are as follows. The piece of aluminium foil containing the americium is dropped into the quartz capsule through a long, narrow glass funnel. The ground glass joint is sealed with high vacuum stop-cock grease. The system is then pumped down to a vacuum of approximately 10^{-6} Torr and thoroughly flamed. The quartz capsule is flamed to the extent that the temperature of the aluminium foil exceeds 500^{o}C so as to remove all traces of atmospheric xenon and krypton surface contamination. Also, flaming of the aluminium foil is necessary to drive off, from the americium, water which, if not removed, might cause a steam explosion during the sealing-off operation. After sufficient flaming of the system, the quartz neck is heated to its melting point, thereby sealing off the capsule. Everything to the left of the dotted line XX is then discarded and replaced with fresh glassware for the next sample.

IRRADIATION OF Am^{241} SAMPLES

Each sample was packed in an aluminium can as shown in Figure 11. It was essential that the flux be accurately known for each irradiation. Therefore, four cobalt monitors were placed in each can, each monitor being a carefully weighed piece of 1% Co, 99% Al alloy.

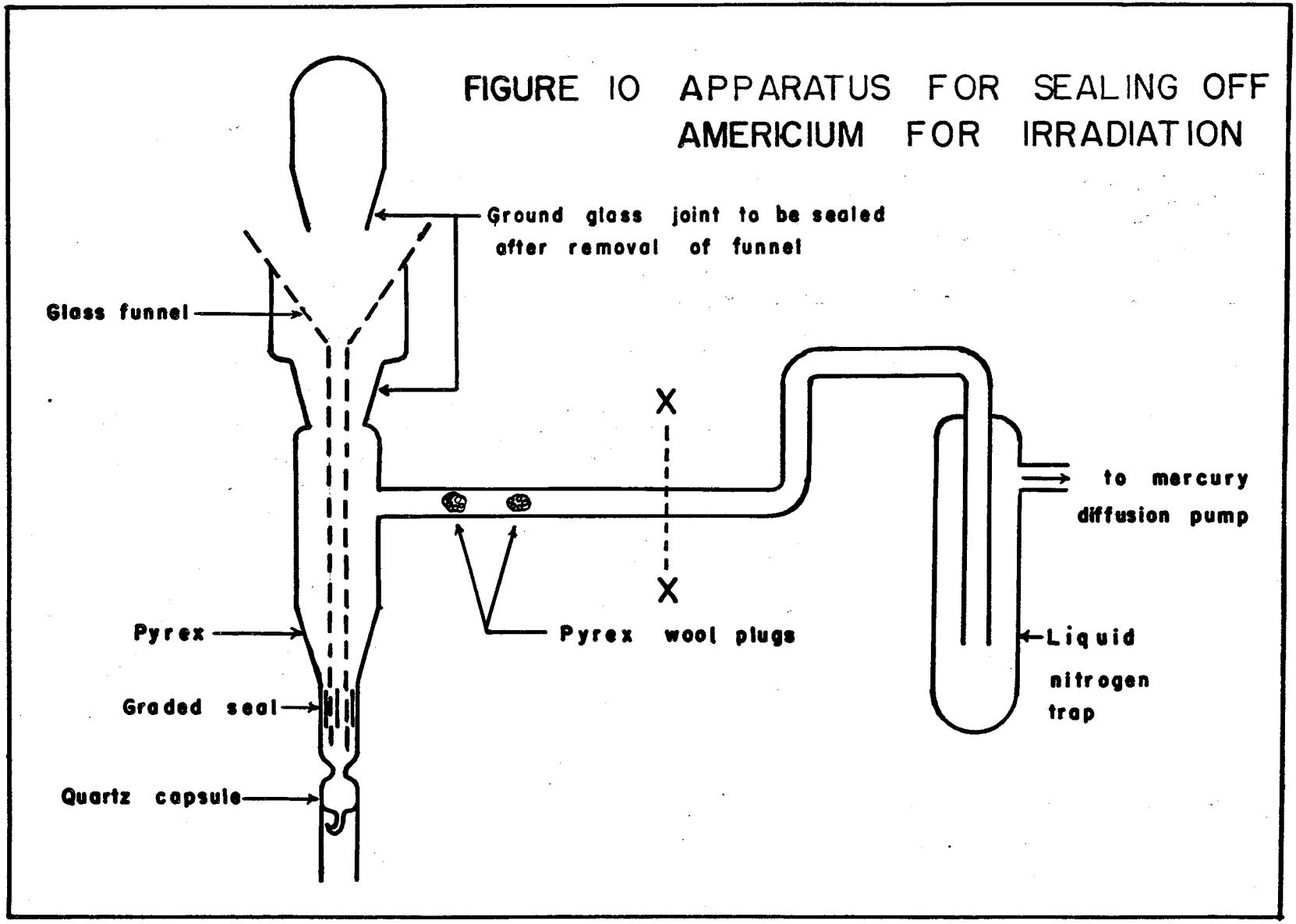
FIGURE 10 APPARATUS FOR SEALING OFF AMERICIUM FOR IRRADIATION
Ground glass joint to be sealed after removal of funnel
Glass funnel
X
X
to mercury diffusion pump
Pyrex
Pyrex wool plugs
Liquid nitrogen trap
Graded seal
Quartz capsule

FIGURE 11 ARRANGEMENT OF COBALT MONITORS

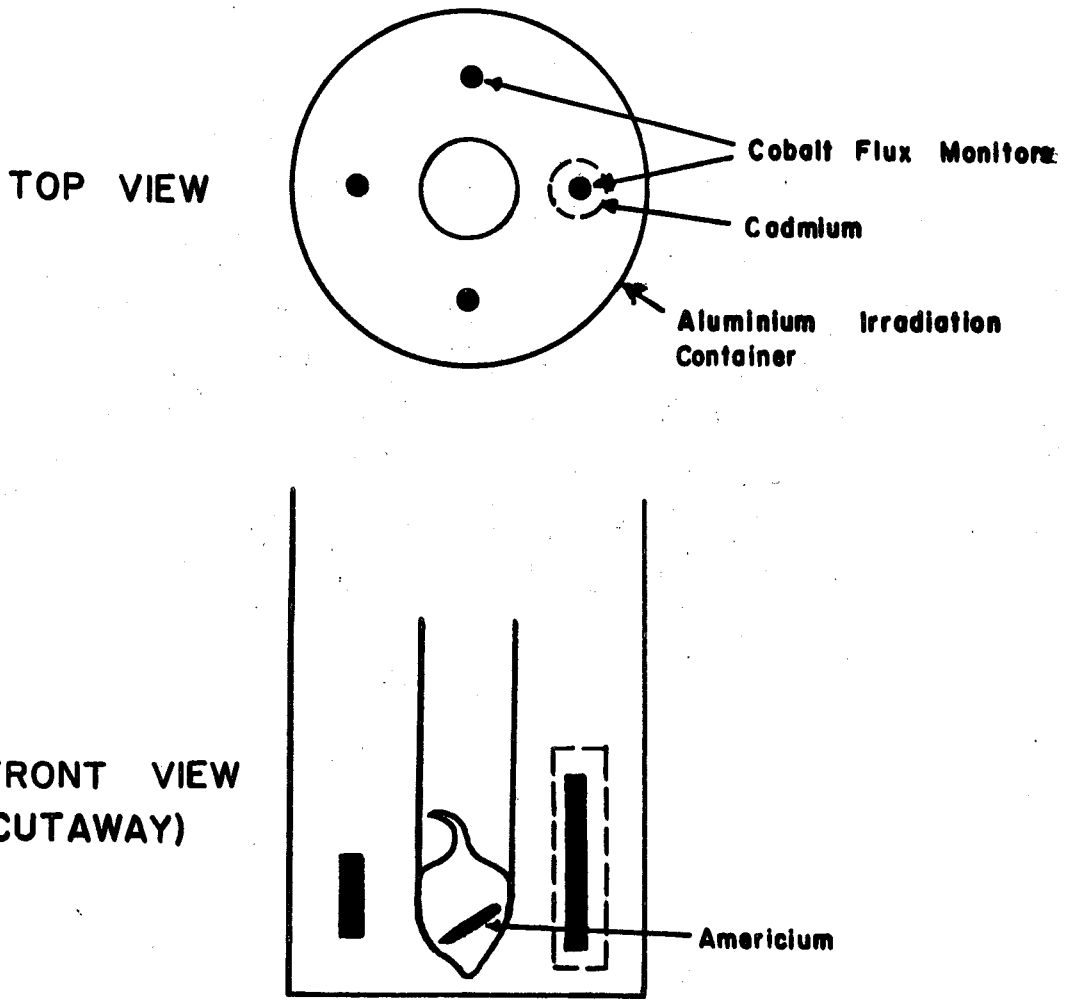

All items are firmly held in position with aluminium foil.

One of the four monitors was wrapped in cadmium to give a measure of the epithermal flux. All samples were irradiated in the McMaster Nuclear Reactor for times ranging from 10 hours to 1000 hours. An additional sample completely surrounded by cadmium together with only one cobalt monitor was irradiated at McMaster for 1000 hours. More irradiation details are given in the chapter entitled RESULTS.

EXTRACTION OF XENON AND KRYPTON FROM IRRADIATED AMERICIUM

The extraction procedure basically consisted of heating the aluminium foil containing the americium to over 800°C and collecting the cooled gases on activated charcoal. The details of the procedure are as follows:

After irradiation, the sample is allowed to cool for a time which is long enough for the precursors of xenon to undergo sufficient β-decay. It is then attached to a vacuum line as shown in Figure 12. The line is first pumped down to a rough vacuum through constriction A_1 and sealed by heating this constriction. Then the mercury float valve V_1 is opened and the line very thoroughly flamed. The purpose of the above sequence of events is to remove as much atmospheric xenon and krypton from the extraction line as possible because the smallest trace of it would seriously contaminate the small amount of fission product xenon and krypton. For this same reason the dimensions of the extraction line should be as small as possible.

After the flaming, V_1 is closed, and the breakseals B_1 and B_2 are broken with the iron breaker (using an external magnet). The activated charcoal C_1 is heated to release accurately known amounts of Kr^{80}, Kr^{82}, and Xe^{128} into the system. (Because these isotopes are scantily produced in fission (48), the addition of this artificial

FIGURE 12 APPARATUS FOR EXTRACTING XENON AND KRYPTON

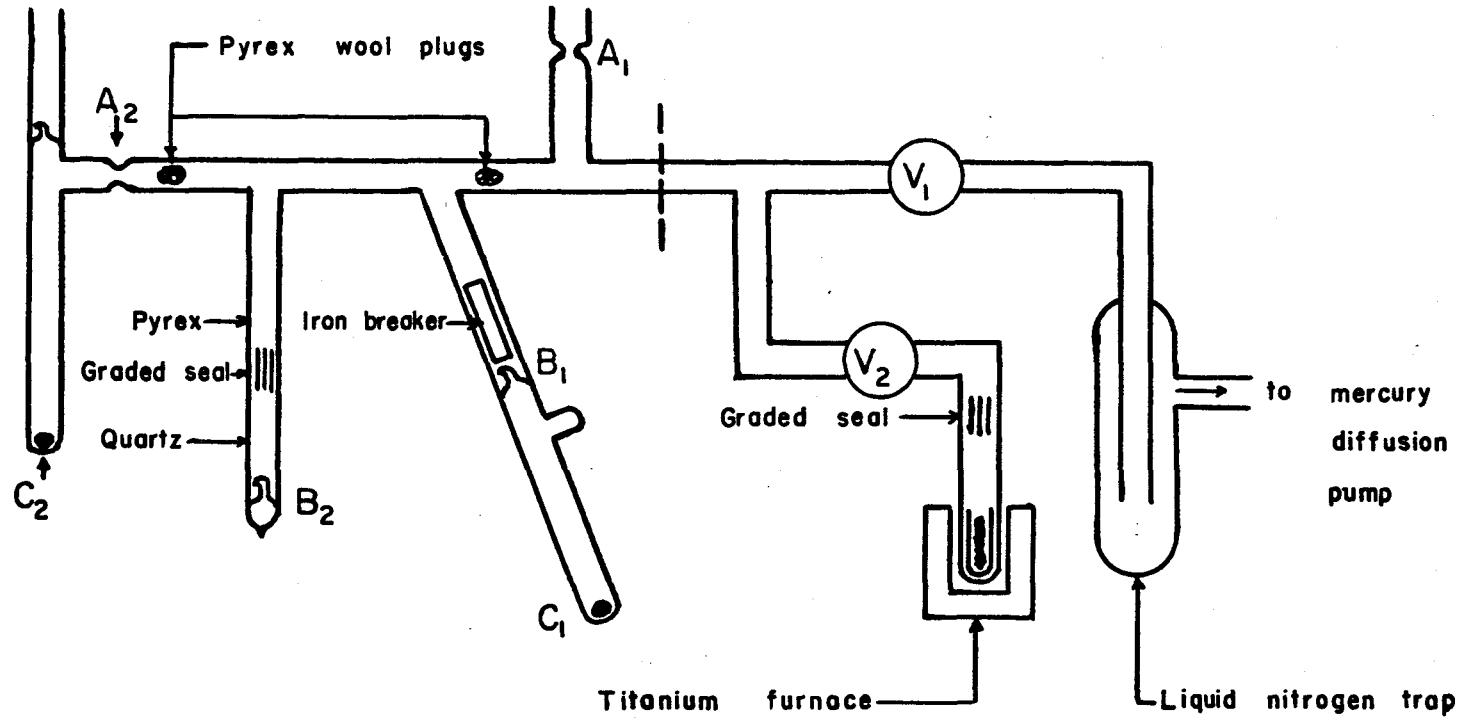

mixture allows an accurate determination of the absolute amounts of the more abundantly produced isotopes in the sample.) The aluminium foil is heated to over 800°C for a 5 minute period or longer. To achieve this temperature, the quartz is heated to over 1100°C. It has been shown (49) for other fissioning nuclides that this heating is sufficient to release at least 99.8% of the fission products that have recoiled into the aluminium foil. The Pyrex wool plugs prevent any americium from reaching A_2 or the dotted line during this heating operation.

In order to remove hydrocarbons and other contaminants that would adversely affect the mass spectrometric analysis, the titanium furnace is heated to 800°C. The mercury float valve V_2 is opened and the Ti is allowed to cool slowly to room temperature for 15 minutes.

Liquid nitrogen is placed around the activated charcoal C_2 and the purified xenon and krypton is allowed to condense for 5 minutes. This is sufficiently long to ensure at least 99.9% condensation. The sample tube can then be sealed and removed by heating constriction A_2 to its melting point. Everything else to the left of the dotted line is discarded according to regulations set down by Atomic Energy of Canada Limited.

MASS SPECTROMETRY

The Mass Spectrometer

The samples were analyzed using a 90°, 10 inch radius, single-focussing mass spectrometer with a resolving power of 600. This instrument and the inlet system are shown schematically in Figure 13. In the ion source, the xenon and krypton are ionized by electron bombardment and accelerated to 2500 ev. After passing through the magnetic analyzer, the ions are further accelerated by a 3000 volt potential difference before striking the first dynode of a 9-stage Cu-Be

electron multiplier. The current from the electron multiplier is amplified by a vibrating reed amplifier and fed to a Leeds and Northrop linear chart recorder. An analysis is done by slowly varying the magnetic field and recording the amplified ion current for each isotope.

Techniques for Analysis of Small Samples

The samples used to measure the fission yields of Am^{241} are extremely small. In some cases the number of atoms per isotope is less than 10^{10}. For samples of this size, the best general procedure is to analyze the krypton first. Valves G_1 and G_2 (see Figure 13) should be kept closed in order to maximize the sensitivity of the mass spectrometer. Then, after releasing the krypton through valves G_1 and G_2, the xenon can be analyzed. The following is a more detailed account of this procedure.

The sample is attached to the inlet system below the mercury float valve V_3 as shown in Figure 13. With the mercury float valves V_1, V_2, V_3, and V_4 open, all parts of the system to the left of L are thoroughly flamed. Then V_1, V_2, V_3, and V_4 are closed; the breakseal B is broken; and V_3 and V_4 are opened again. The activated charcoal C_2 is heated to $100^{\circ}C$ to release the sample into the bowl. V_3 and V_4 are then closed and liquid air is placed on the trap T to hold back all of the xenon while the krypton is entering the mass spectrometer. The mercury is then raised to the top of the bowl and the ground glass ball and cup valves G_1 and G_2 are closed. The krypton is allowed to enter for 15 minutes through the leak L. Then the xenon and the remaining krypton are condensed onto the activated charcoal C_1 by opening V_2 and V_4 while C_1 is surrounded by liquid air and T is heated to room temperature.

About 10% of the original krypton is now trapped in the mass

FIGURE 13 MASS SPECTROMETER AND INLET SYSTEM

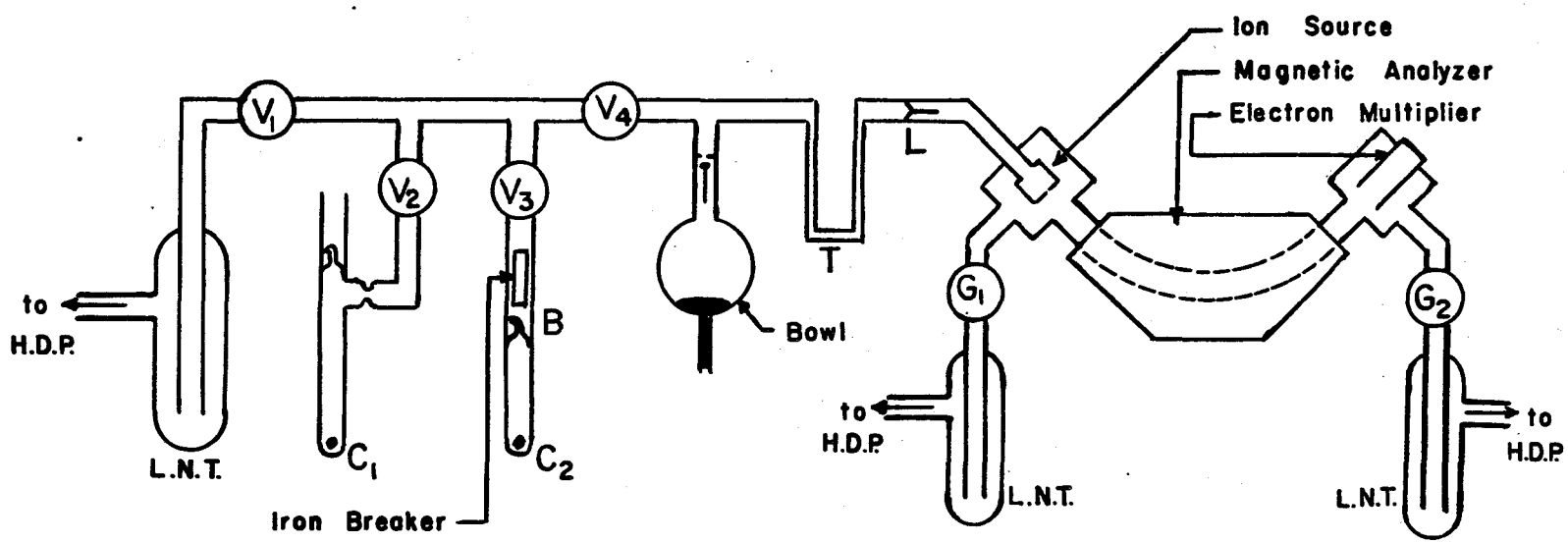

H.D.P. — Hg Diffusion Pump
L.N.T. — Liquid Nitrogen Trap

spectrometer between L, G_1, and G_2. It is analyzed by slowly increasing the magnet current so that the ion beam for each isotope slowly crosses the slit in front of the electron multiplier. In order to save time, the region between peaks is scanned very quickly. When the end of the krypton mass region is reached the scanning is repeated in the opposite direction. This sequence, known as a run, is repeated 6 to 8 times. Using this quick-scan technique, one run can be made in 8 minutes. A typical half-run is shown in Figure 14. It is extremely important that each run be made as quickly as possible because the sample in the mass spectrometer tends to diminish in size as a result of adsorption on the surfaces and leakage through G_1 and G_2. The depletion rate is 50% in 70 minutes.

Analyzing with G_1 and G_2 closed is referred to as static analysis as opposed to dynamic analysis in which G_1 and G_2 are kept open so that the sample is pumped away instead of being allowed to recirculate. During a dynamic analysis, the sample continually enters the mass spectrometer through leak L. The static method has the advantage of giving a 50-fold increase in sensitivity. The dynamic method has the advantage of preventing a memory effect. This latter effect will be discussed more thoroughly in the section on "Source of Error". A compromise between the static and dynamic system can be achieved by closing G_1 but leaving G_2 open. This is referred to as semi-static analysis. It is 8 times more sensitive than dynamic analysis and is much less susceptible to memory effect than is static analysis. For these reasons, the larger samples of xenon were analyzed by this method.

Before analyzing the xenon, V_1, V_4, G_1, and G_2 are opened with V_2 and V_3 closed. This is to remove any xenon which may have been released from the walls of the mass spectrometer during the krypton

FIGURE 14 TYPICAL CHART RECORD OF FISSION-PRODUCT KRYPTON ISOTOPE ABUNDANCES

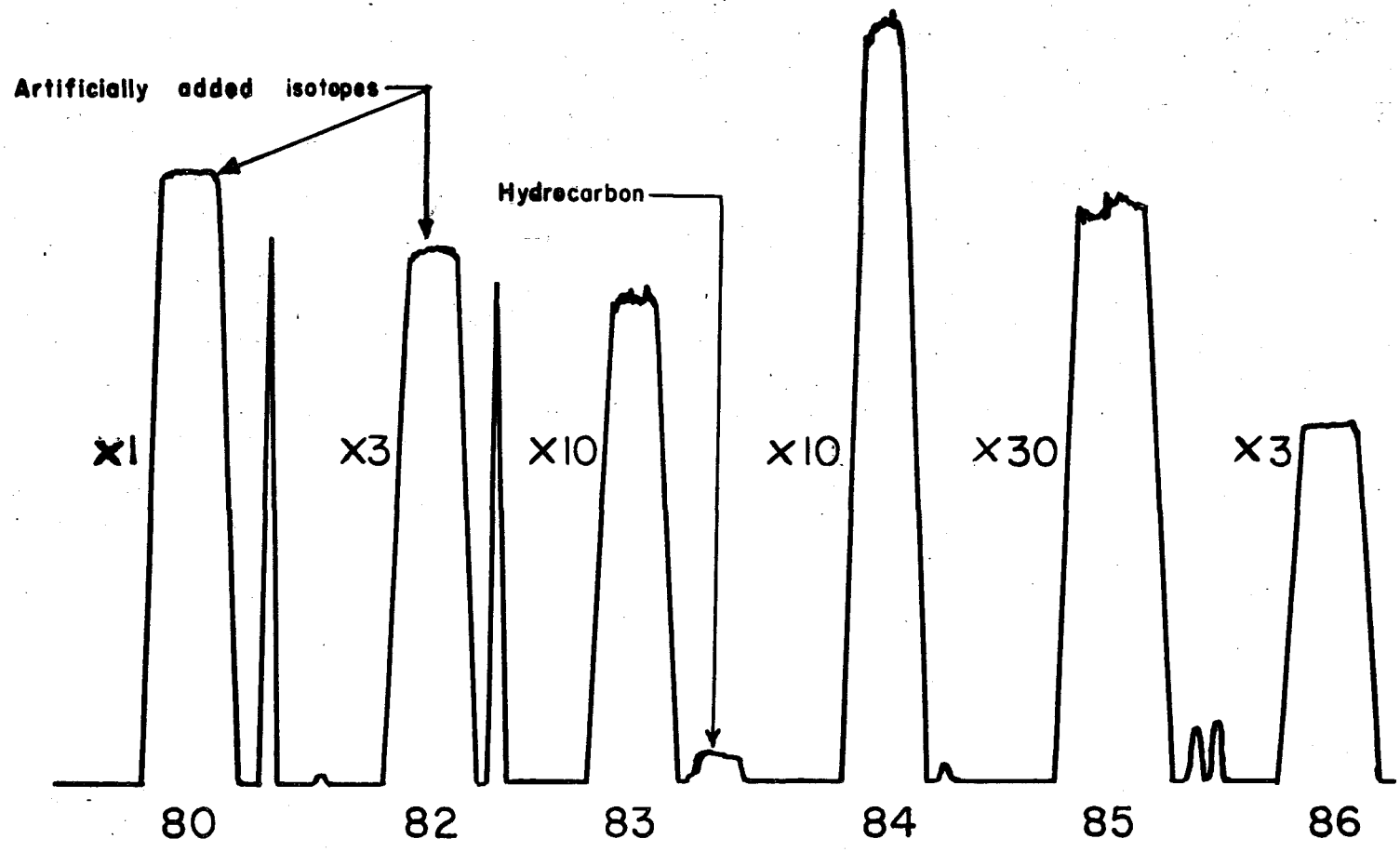

analysis. After a wait of 10 minutes, the xenon in the sample can be analyzed either statically or semi-statically depending on the size of the sample. A typical half-run is shown in Figure 15, this time scanning in the opposite direction to that in Figure 14. After analysis, the remainder of the sample can be condensed on the charcoal C_1, sealed off, and saved for future use.

Sources of Error

(a) Hydrocarbons

Hydrocarbons occur at every mass number and are approximately 0.17% heavier than the corresponding monatomic gases such as xenon and krypton. Therefore, the mass spectrometer's resolving power of 600 is sufficient to separate the hydrocarbons from xenon and krypton. However, if the sample is extremely small, the tails of the hydrocarbon peaks interfere with the precise measurement of the xenon and krypton peaks.

In order to lower the hydrocarbon background to a tolerable level, the source and detector assemblies are baked at 400°C for three days after the mass spectrometer has been pumped down from atmospheric pressure. Other parts of the mass spectrometer are thoroughly flamed. Figure 14 shows a hydrocarbon that was accidentally included in the scanning. Other hydrocarbons are shown in Figure 15. The sample for these scans was about 9 times larger than the smallest sample. It can be seen that the hydrocarbon background was low enough so that it did not interfere with any measurements except those of Xe^{130} and atmospheric Xe^{129}.

(b) Atmospheric Contamination

With very small samples, atmospheric contamination can be a

FIGURE 15 TYPICAL CHART RECORD OF FISSION-PRODUCT XENON ISOTOPE ABUNDANCES

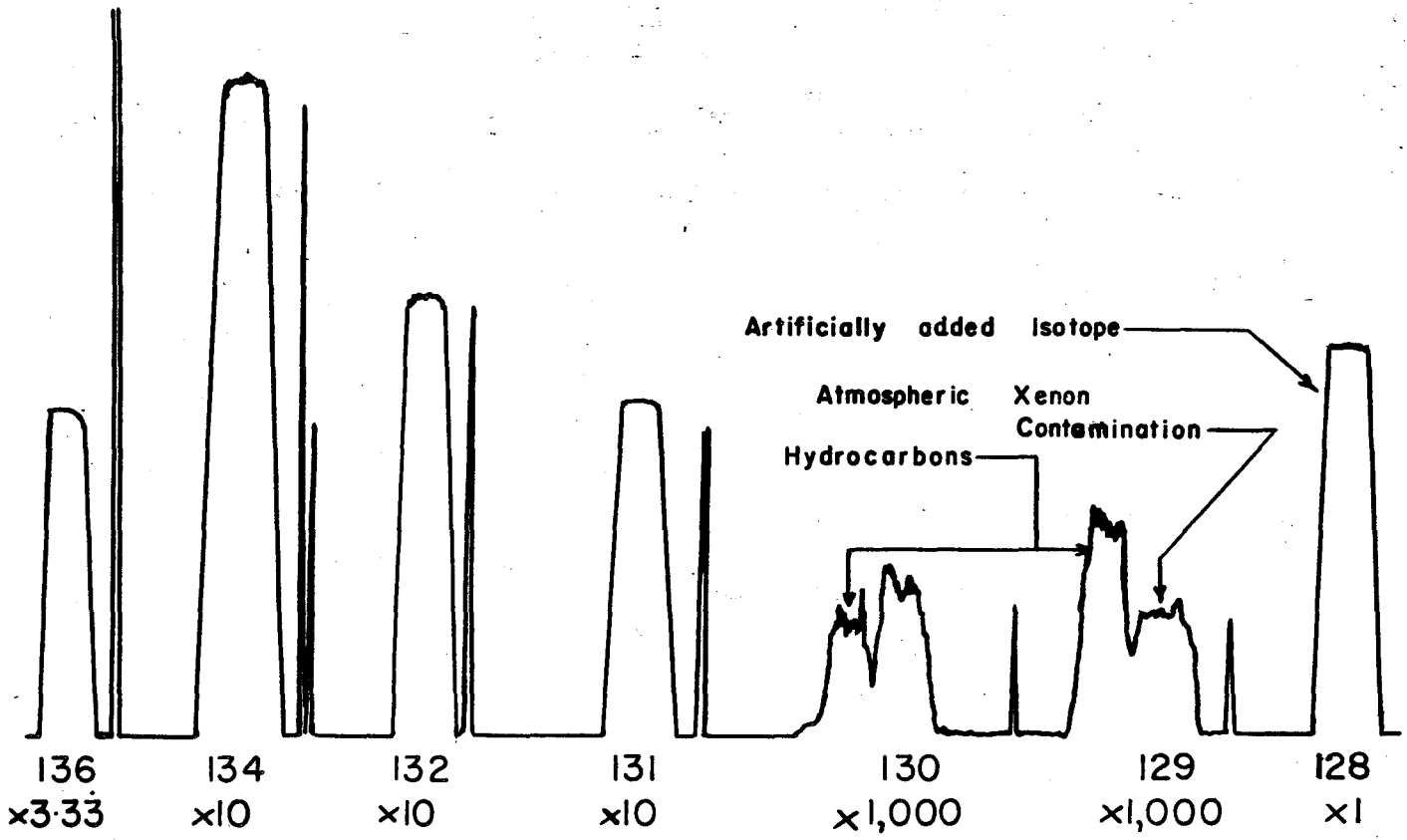

serious problem. As mentioned in the sections on sample preparation and extraction, every effort is made to prevent contamination of the sample itself. Also, the mass spectrometer and the inlet system must be freed of contamination. This is accomplished by the procedure for removing hydrocarbons from the mass spectrometer (see subsection (a)) and also by thorough flaming of the inlet system. Even the most exhaustive efforts will leave measurable amounts of xenon and krypton. Fortunately, there is no Xe^{129} in freshly prepared fission product samples because the 129 mass chain is held up by 1.6×10^{7}-year I^{129}. Therefore, any Xe^{129} measured during an analysis is entirely due to atmospheric contamination. Because the isotopic composition of atmospheric xenon is well known, the amount of atmospheric contamination of the fission-produced isotopes can be calculated.

Corrections for atmospheric krypton can also be made. In small samples, the amount of fission-product Kr^{80} and Kr^{82} will be negligible compared to the amount of atmospheric Kr^{80} and Kr^{82}. If an artificial mixture of Kr^{80} and Kr^{82} is added to the sample, as was done for the americium samples, then the deviation of the Kr^{80}/Kr^{82} ratio from that of the original artificial mixture will indicate the amount of atmospheric contamination.

(c) Memory Effect

While a sample is being analyzed, some of the ions which bombard the analyzer tube and the ion collector remain embedded in the metal. When the next sample is run, this embedded xenon and krypton is released by ion bombardment, thereby contaminating the sample. This problem is known as memory effect and is especially serious if the static method of analysis is being used. It can be effectively eliminated by passing neon through the mass spectrometer for 12 hours with the ion source turned on. The bombardment with neon ions

removes the embedded xenon and krypton so that the memory effect is negligible in the next sample.

(d) Mass Discrimination and Fractionation

Mass discrimination may occur at the electron multiplier if the average number of secondary electrons per incident ion varies with the ion mass. Fractionation of the sample may occur at leak L and valves G_1 and G_2. These systematic errors are difficult to calculate but they can easily be checked by running samples of atmospheric xenon and krypton of which the isotopic compositions are well known. This was done using the same procedures of analysis as were used for the americium samples, and it was found that the deviations from the accepted values were less than 1%.

RESULTS

CUMULATIVE YIELDS IN THE XENON MASS REGION

The relative yields of the 131, 132, 134, and 136 mass chains as determined from the measured Xe ratios are shown in Table 1. Corrections have been made for normal contamination in all samples and for the decay of 8.05 day I^{131} and 77.8 hour Te^{132} in samples 6 and 7 which were extracted less than four weeks after irradiation. In all other samples shown in the table, a correction for I^{131} decay would have been much less than the precision of the measurement. In order to determine the yield of the 136 mass chain, it was also necessary to correct for the neutron capture of Xe^{135} and for the independent yield of Cs^{136} measured by Rickard et al. (45). The corrections for the 136 mass chain are explained in detail in Appendix I.

The yields given in Table 1 are for various combinations of Am^{241}, Am^{242}, and Am^{242m}. Using the cross-sections listed in Table 2, the relative numbers of fissions of these isotopes have been calculated according to the equations:

$$\frac{N_f(242)}{N_f(241)} = \frac{\sigma_{c1}\,\sigma_{242f}\,\Phi}{\sigma_{241f}\,\lambda}\left[\frac{t-(1/\lambda)(1-e^{-\lambda t})}{t}\right] \quad . \quad . \quad . \quad . \quad 3$$

and

$$\frac{N_f(242m)}{N_f(241)} = \frac{\sigma_{c2}\,\sigma_{242*f}}{\sigma_{cf}\,\sigma_{241f}}\left[1-\frac{(1-e^{-\Phi\sigma_{cf}t})}{\Phi\sigma_{cf}t}\right] \quad . \quad . \quad . \quad . \quad 4$$

where $N_f(242)$ = number of fissions of 16.0 hour Am^{242}

$N_f(241)$ = number of fissions of Am^{241}

σ_{c1} = neutron capture cross-section of Am^{241} leading to production of 16.0 hour Am^{242}

TABLE 1

Relative Yields in Xenon Mass Region

Sample No.	Flux (neutrons/cm.^{2}-sec.)	Irradiation Time (hours)	Cadmium Ratio	$\frac{Y_{131}}{Y_{132}}$	$\frac{Y_{134}}{Y_{132}}$	$\frac{Y_{136}}{Y_{132}}$
1	$(1.06 \pm 3) \times 10^{13}$	1000	17.4	0.732 ± 3	1.562 ± 2	1.86 ± 10
2	$(1.05 \pm 3) \times 10^{13}$	503.6	20.2	0.735 ± 4	1.577 ± 3	1.85 ± 9
3	$(8.24 \pm 22) \times 10^{12}$	275	20.5	0.738 ± 8	1.558 ± 8	1.74 ± 10
4	$(1.17 \pm 4) \times 10^{13}$	100	14.9	0.740 ± 5	1.546 ± 5	1.58 ± 10
5	$(7.83 \pm 39) \times 10^{12}$	75	24.5	0.748 ± 4	1.524 ± 11	1.71 ± 7
6	$(1.39 \pm 4) \times 10^{13}$	20	13.9	0.744 ± 5	1.513 ± 8	1.65 ± 6
				0.742 ± 4	1.521 ± 3	1.66 ± 5
7	$(1.46 \pm 6) \times 10^{13}$	10	10.7	0.745 ± 2	1.515 ± 6	1.63 ± 3
				0.745 ± 4	1.522 ± 7	1.64 ± 3

TABLE 2

Cross Sections

Neutron Capture:

Am^{241} to 16.0 hr. Am^{242}	....	600 ± 100	barns
Am^{241} to 152 yr. Am^{242m}	....	50 ± 10	barns
Am^{242m} to Am^{243}	....	5500 ± 500	barns

Fission:

Am^{241}	....	3.13 ± 0.15	barns
Am^{242} (16.0 hr.)	....	2500 ± 500	barns
Am^{242m} (152 yr.)	....	6400 ± 500	barns

σ_{242f} = fission cross-section of 16.0 hour Am^{242}

σ_{241f} = fission cross-section of Am^{241}

φ = neutron flux

λ = decay constant of 16.0 hour Am^{242}

t = irradiation time

$N_f(242m)$ = number of fissions of (152 year) Am^{242m}

σ_{c2} = neutron capture cross-section of Am^{241} leading to the production of Am^{242m}

σ_{242*f} = fission cross-section of Am^{242m}

σ_{cf} = the sum of the fission and neutron capture cross-sections of Am^{242m}

The derivation of these equations is given in Appendix II. The irradiation of samples 1 and 2 was interrupted several times and it was necessary to correct for these interruptions when using equation 3. The results of these calculations are summarized in Table 3.

The yield values in Table 1 are plotted against the fraction of the fissions which is due to Am^{242} and Am^{242m} in Figures 16, 17, and 18. By extrapolating these curves to the left where the Am^{242}/Am^{241} fission ratio is zero, the yield ratios for pure Am^{241} fission can be deduced. This has been done and results are shown in Table 4.

The problem of determining the Am^{242} yields by extrapolation in the other direction is much more complicated. This is because the cross-sections in equations 3 and 4 are not accurately known. Nevertheless, the Am^{242} yields can be estimated although the limits of error are much wider than for Am^{241}. This has been done in Table 5.

It should be noted that the large uncertainties in the cross-sections have little effect on the precision of the Am^{241} yield measurements. This is because the uncertainties affect only the coefficient in front of the brackets in equations 3 and 4 for the shorter irradiations.

TABLE 3

Fission Ratios

Sample No.	Irradiation Time (hours)	No. of fissions of 16.0 hr. Am^{242} / No. of fissions of Am^{241}	No. of fissions of 152 yr. Am^{242m} / No. of fissions of Am^{241}	No. of fissions of Am^{242} and Am^{242m} / Total no. of fissions
1	1000	0.384	1.690	0.675
2	503.6	0.388	0.907	0.564
3	275	0.302	0.404	0.414
4	100	0.361	0.212	0.364
5	75	0.220	0.108	0.247
6	20	0.183	0.051	0.190
7	10	0.108	0.027	0.119

FIGURE 16 DEPENDENCE OF 131/132 YIELD RATIO ON GROWTH OF Am^{242} AND Am^{242m}

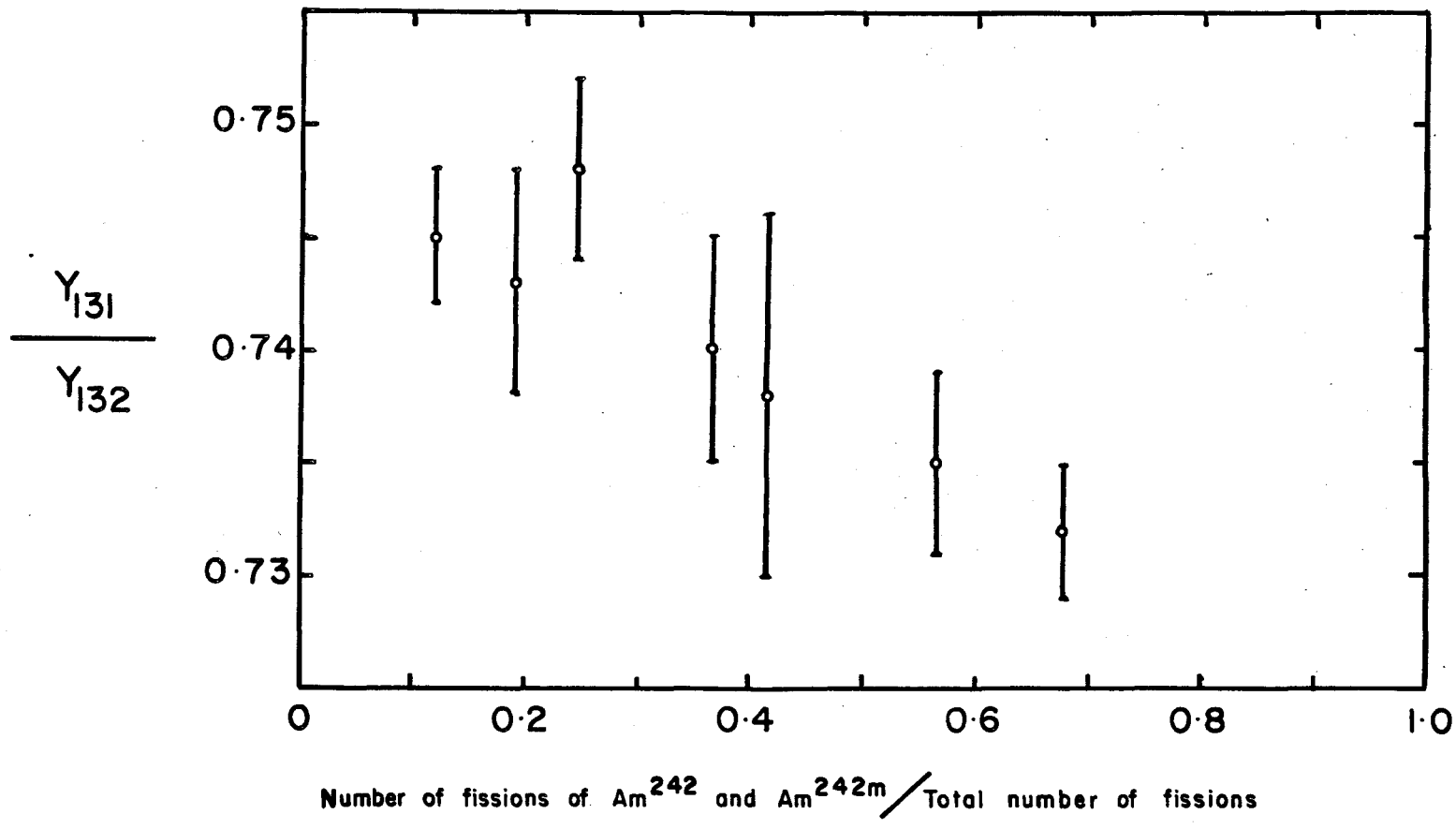

FIGURE 17 DEPENDENCE OF 134/132 YIELD RATIO ON GROWTH OF Am^{242} AND Am^{242m}

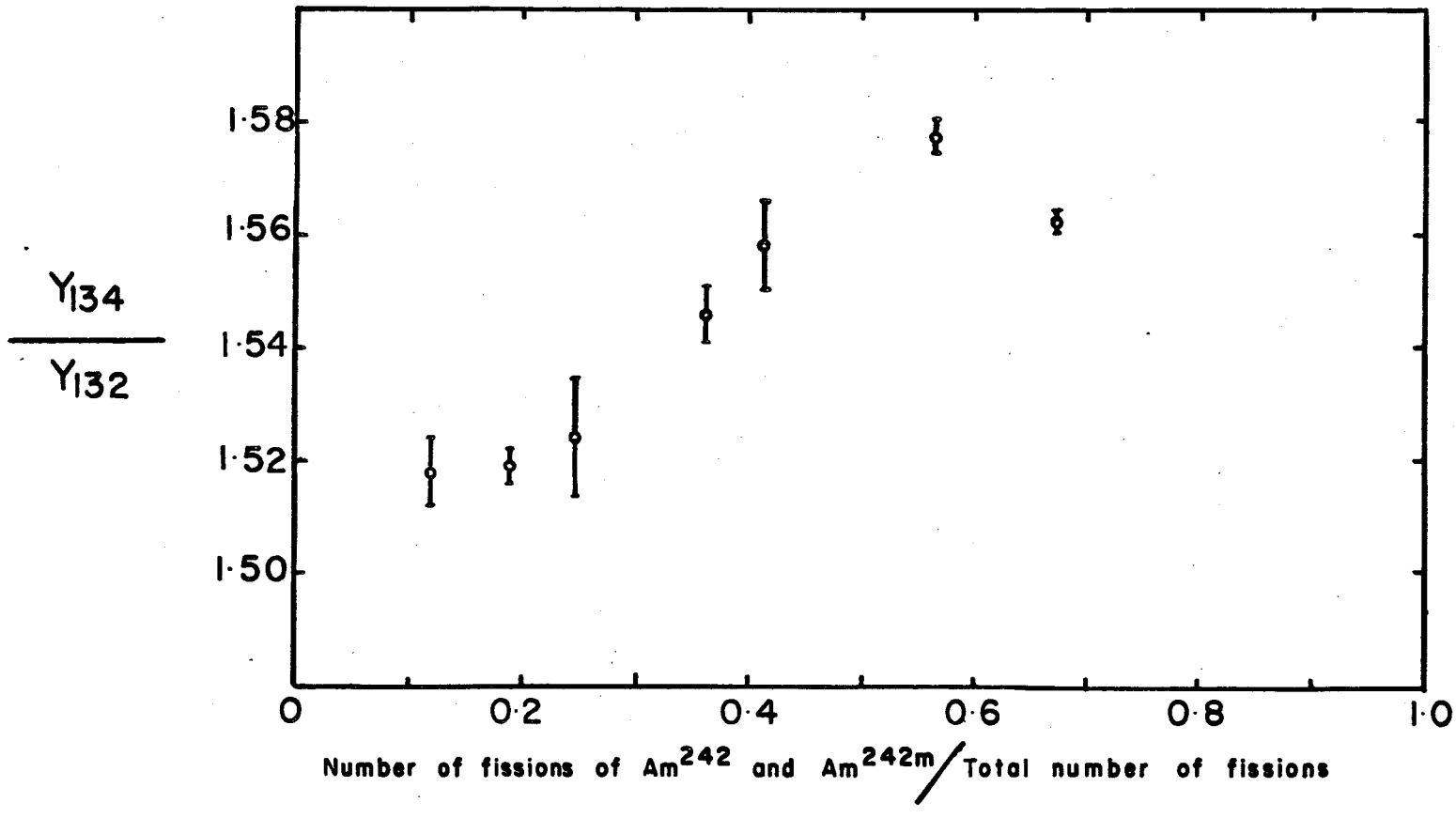

FIGURE 18 DEPENDENCE OF 136/132 YIELD RATIO ON GROWTH OF Am^{242} AND Am^{242m}

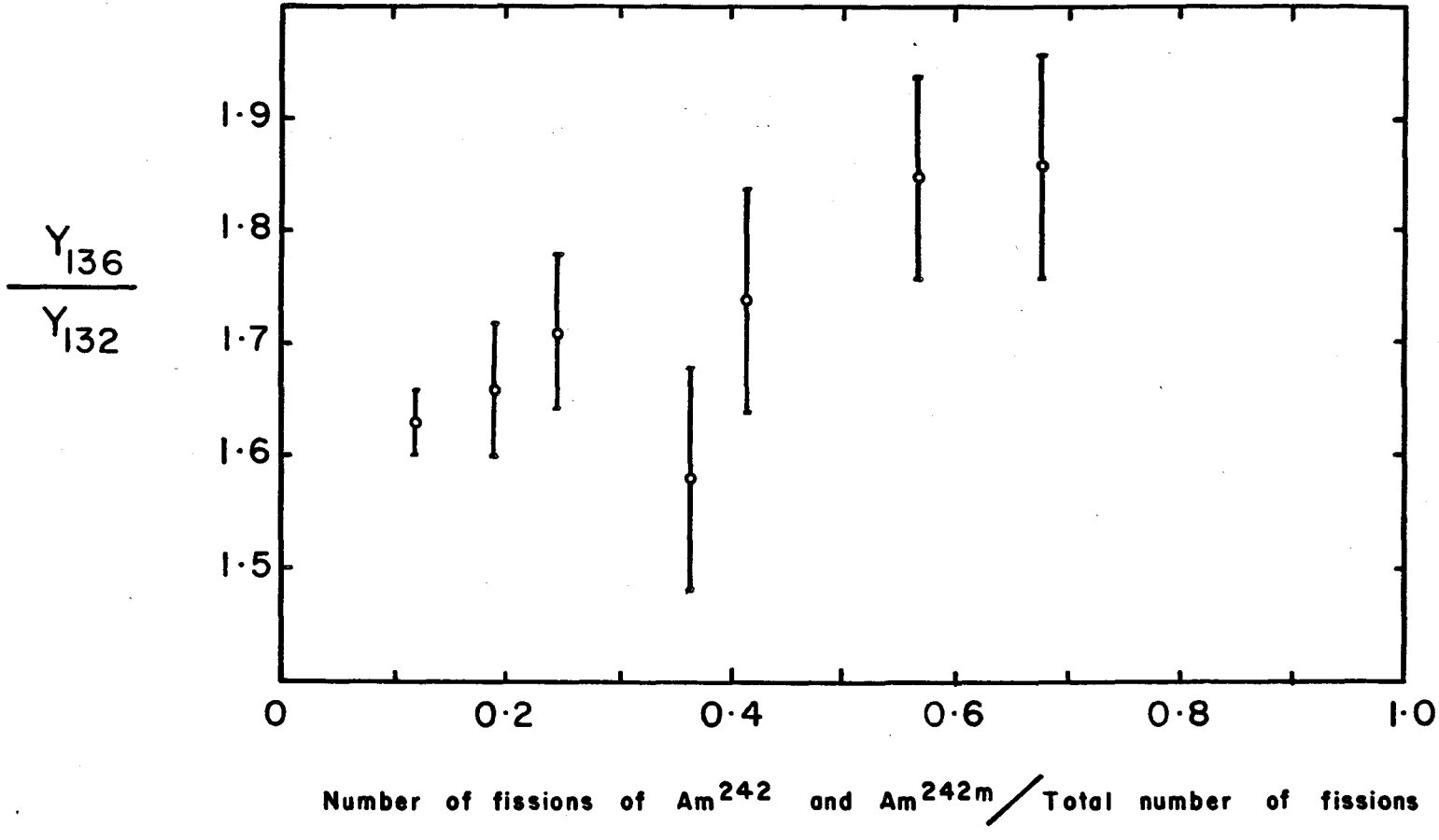

TABLE 4

Relative Yields of Am^{241} in the Xenon Mass Region

Mass Chain	Yield Relative to Xe^{132} Yield
131	0.747 ± 0.003
132	1.000
134	1.52 ± 0.01
136	1.60 ± 0.03

TABLE 5

Relative Yields of Am^{242} in the Xenon Mass Region

Mass Chain	Yield Relative to Xe^{132} Yield
131	0.725 ± 0.005
132	1.000
134	1.6 ± 0.1
136	1.9 ± 0.1

Even if the cross-sections are not well known, at least they will not vary from sample to sample. If the relative fluxes and the irradiation times are accurately known, the backward extrapolation of the yield curves will give essentially the same results even if all of the cross-section values used in the equations are altered by as much as 20% each.

Samples 6 and 7 were each analyzed by the static method using two separate fractions (a) and (b). The self-consistency of the measurements indicates that sample depletion is not a large source of error.

It can be seen in Table 1 that the precision of the 131/132 and 134/132 yield ratios is much better than that of the 136/132 ratios. In the former case, the principal source of error is the variation of the measured xenon ratio from one run to another. The quoted error is the root mean square deviation of the ratio for the individual runs from the average ratio for all of the runs. It has been found in the past that the precision of measuring atmospheric xenon ratios is best represented in this way.

The principal source of error in the 136/132 ratio is the correction for the neutron capture of Xe^{135}. The radiochemically-determined yield of Xe^{135} (45) was used in the calculation of this correction and, therefore, the error associated with this yield is more strongly reflected in the samples which were irradiated for longer times since it is in these samples that the effect of "Xe^{135} burn-up" is greater. Therefore, the precision of the Am^{241} yield measurements is less adversely affected by this correction than the precision of the Am^{242} yield measurements.

The flux for each sample was determined by measuring the specific activity of each cobalt monitor in an ionization chamber. Since there were three widely-spaced cobalt monitors per sample (which were not wrapped in cadmium) the flux distribution in each irradiation can

could also be determined. The fluxes given in Table 1 are the averages for each set of three monitors and the quoted errors are mainly an indication of the flux distribution. The absolute values of the fluxes were determined by calibrating the ionization chamber with three cobalt samples of known activities. The error in calibration was included in the estimated error.

A fourth cobalt monitor in each irradiation can was wrapped in cadmium and its specific activity relative to that of the unwrapped monitors gave a measure of the epithermal flux. The ratio of the specific activity of an unwrapped flux monitor to that of a cadmium-wrapped monitor is commonly called a cadmium ratio. The cadmium ratio for each sample is given in Table 1.

Errors in the absolute values of the Am^{242}/Am^{241} fission ratios given in Table 3 are quite large because of the large uncertainties in the cross-sections. However, errors in the relative values are much smaller and are mainly the result of errors in the flux determination. To avoid a misleading representation, the errors are not listed in this Table but are taken into account in Tables 4 and 5.

INDEPENDENT YIELDS OF I^{130}

The independent yields of I^{130} which decays to stable Xe^{130} are given in Table 6. The mass spectrometer was operating at its limit of sensitivity for these measurements. A very large correction for atmospheric xenon was necessary for the smaller samples.

CUMULATIVE YIELDS IN THE KRYPTON MASS REGION

The relative yields of the 83, 84, 85, and 86 mass chains as indicated by the measured krypton ratios are shown in Table 7. The 85 mass chain decays through krypton according to the following decay

TABLE 6

Independent Yield of I^{130} Relative to 132 Mass Chain Yield

Sample Number	Irradiation Time (hours)	Measured Ratio of Xe^{130}/Xe^{132} (corrected for atmospheric contamination)
1	1000	$(1.90 \pm 0.10) \times 10^{-3}$
2	503.6	$(2.48 \pm 0.05) \times 10^{-3}$
3	275	$(2.46 \pm 0.12) \times 10^{-3}$
4	100	$(2.94 \pm 0.15) \times 10^{-3}$
5	75	$(2.89 \pm 0.08) \times 10^{-3}$
6	20	$(3.0 \pm 0.3) \times 10^{-3}$
		$(3.0 \pm 0.4) \times 10^{-3}$
7	10	unmeasurable
8	1000 (Cadmium-wrapped)	$(6.2 \pm 0.3) \times 10^{-3}$

TABLE 7

Relative Yields in Krypton Mass Region

Sample No.	Flux (neutrons/cm.^{2}-sec.)	Irradiation Time (hours)	Cadmium Ratio	$\frac{Y_{83}}{Y_{84}}$	$\frac{Y_{85}}{Y_{84}}$	$\frac{Y_{86}}{Y_{84}}$
1	$(1.06 \pm 3) \times 10^{13}$	1000	17.4	0.267	0.183	0.512
2	$(1.05 \pm 3) \times 10^{13}$	503.6	20.2	0.657	1.136	1.557
3	$(8.24 \pm 22) \times 10^{12}$	275	20.5	0.669	1.157	1.611
4	$(1.17 \pm 4) \times 10^{13}$	100	14.9	0.656	1.139	1.520
5	$(7.83 \pm 39) \times 10^{12}$	75	24.5	0.651	1.121	1.491
6	$(1.39 \pm 4) \times 10^{13}$	20	13.9	0.654	1.127	1.514
7	$(1.46 \pm 6) \times 10^{13}$	10	10.7	0.628	1.075	1.440

scheme.

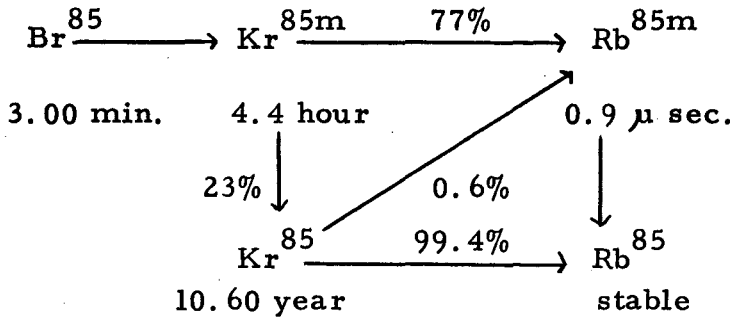

Corrections were made for the Kr^{85m} branching ratio and for the decay of 10.60 year Kr^{85}. No corrections were made for atmospheric contamination because the ratio of the amount of fission product krypton to the amount of artifically-added Kr^{80} and Kr^{82} was too small. Variations in the measured Kr^{80}/Kr^{82} ratio were too small to indicate the presence of atmospheric contamination even though there may have been a significant amount relative to the fission-produced krypton. However, samples 2 to 7 inclusive showed little variation in the fission product krypton ratios even though the amount of atmospheric xenon contamination varied over several orders of magnitude. It is probable that the atmospheric krypton contamination also varied over several orders of magnitude. Because the atmospheric isotope abundance pattern (measured by Neir (50)) is very different from the measured krypton isotope patterns (see Table 7) one would expect large variations in the measured ratios from one sample to another if any of the samples was seriously contaminated. Therefore, one can safely assume that there was only a slight contamination in samples 2 to 7. An example of a seriously-contaminated sample is sample 1 which has been included in Table 7 for illustrative purposes only.

However, the slight atmospheric contaminations which could not be measured masked any small differences which might have existed between the krypton yield patterns for Am^{241} and Am^{242}. Nevertheless,

the yields for both of these nuclides can be estimated within limits of error determined by possible atmospheric contamination and uncertainties of cross-sections used in equations 3 and 4. These results are given in Table 8.

RATIO OF XENON TO KRYPTON

The ratio of the amount of fission-produced Xe^{132} to the amount of fission-produced Kr^{85} was accurately determined for each sample. This was accomplished using the known amounts of Kr^{80}, Kr^{82}, and Xe^{128} in each sample according to the following equation.

$$\left[\frac{Xe^{132}}{Kr^{85}}\right] = \left[\frac{Xe^{132}}{Xe^{128}}\right]\left[\frac{Xe^{128}}{Kr^{80}}\right]\left[\frac{Kr^{80}}{Kr^{85}}\right]$$

The Xe^{132}/Xe^{128} ratio was measured and corrected for atmospheric contamination in each sample. The Xe^{128}/Kr^{80} was determined separately using a standard mixture of atmospheric xenon and krypton and was the same for all samples. The Kr^{80}/Kr^{85} ratio was measured for each sample and corrected for Kr^{85} branching and decay and for atmospheric contamination using the measured Kr^{80}/Kr^{82} ratio. The results are given in Table 9.

The accurate determination of these ratios would have been impossible without the addition of the Kr^{80}, Kr^{82}, and Xe^{128} mixture. This is because the relative sensitivity of the mass spectrometer for xenon with respect to krypton is dependent on many electrical parameters in the source and ion detector. These parameters are altered slightly from sample to sample in order to optimize the precision of measurement. Therefore, although the addition of Kr^{80}, Kr^{82}, and Xe^{128} lowered the accuracy of the 83, 84, 85, and 86 mass chain yield measurements relative to each other by preventing a correction for atmospheric krypton contamination, it nevertheless permitted the acquisition of otherwise

TABLE 8

Relative Yields of Am^{241} and Am^{242} in Krypton Mass Region

	Mass Chain	Yield Relative to Kr^{84} Yield
Am^{241}	83	0.65 ± 0.04
	84	1.000
	85	1.13 ± 0.11
	86	1.52 ± 0.18
Am^{242}	83	0.65 ± 0.06
	84	1.000
	85	1.1 ± 0.2
	86	1.5 ± 0.3

TABLE 9

Xenon-Krypton Ratios

Sample Number	Irradiation Time (hours)	$\frac{Y_{132}}{Y_{85}}$
1	1000	9.4 ± 0.4
2	503.6	10.3 ± 0.4
3	275	9.2 ± 0.4
4	100	9.6 ± 0.3
5	75	10.0 ± 0.3
6	20	9.8 ± 0.4
7	10	8.5 ± 0.4

unobtainable data.

FISSION INDUCED BY EPITHERMAL NEUTRONS

Sample 8 was surrounded by a cadmium container of wall thickness 0.8 mm. As a result, the fissions were induced mainly by epithermal neutrons. The data obtained from analysis of this sample are summarized in Table 10.

ABSOLUTE FISSION YIELDS

In order to convert the relative yields for Am^{241} fission to absolute yields, the results were normalized to the radiochemically-determined absolute yield of the 133 mass chain (45). The final decays of the 133 mass chain are

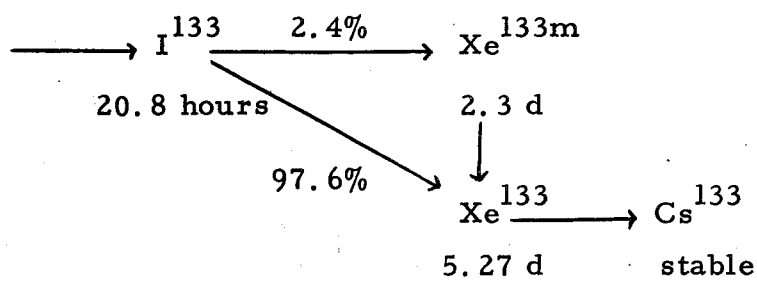

However, before this normalization could be accomplished, it was necessary to measure the Xe^{133}/Xe^{134} ratio mass spectrometrically at a particular time after irradiation. Sample 9 was irradiated for 10 hours; the xenon and krypton were extracted 133 hours after the end of the irradiation; and the Xe^{133}/Xe^{134} ratio was measured 71 hours after extraction. Corrections were made for atmospheric contamination and for the decay of I^{133}, Xe^{133m}, and Xe^{133}. The data associated with the analysis of sample 9 are given in Table 11. The results of the normalization are given in Table 12. The errors in Table 12 are largely due to the 5% error reported by Rickard et al. (45) for the 133 chain yield.

TABLE 10

Relative Yields for Am^{241} Fission Induced by Epithermal Neutrons

Sample Number: 8

Irradiation Time: 1000 hours

Epithermal Flux: $(7.6 \pm 0.3) \times 10^{11}$ neutrons/cm.^{2}-sec.

$\frac{Y_{83}}{Y_{84}}$: 0.677 ± 0.003

$\frac{Y_{85}}{Y_{84}}$: 1.167 ± 0.006

$\frac{Y_{86}}{Y_{84}}$: 1.533 ± 0.007

$\frac{Y_{131}}{Y_{132}}$: 0.763 ± 0.003

$\frac{Y_{134}}{Y_{132}}$: 1.463 ± 0.011

$\frac{Y_{136}}{Y_{132}}$: 1.483 ± 0.010

TABLE 11

Determination of Relative Yield of 133 Mass Chain for Am^{241} Fission

Sample Number: 9

Irradiation Time: 10 hours

Flux: $(1.47 \pm 0.02) \times 10^{13}$ neutrons/cm.^{2}-sec.

Cadmium Ratio: 12.5

Time between End of Irradiation and Extraction: 133 hours

Time between Extraction and Analysis: 71 hours

$\frac{Y_{133}}{Y_{134}}$: 0.759 ± 0.007

TABLE 12

Absolute Yields of Am^{241} in Xenon Mass Region

Mass Chain	Absolute Yield %
131	2.6 ± 0.2
132	3.5 ± 0.2
133	4.0 ± 0.2
134	5.3 ± 0.3
136	5.6 ± 0.4

COMPARISON WITH RADIOCHEMICAL YIELDS

Three of the mass chain yields measured in these experiments for Am^{241} had been recently measured radiochemically by Rickard et al. (45). These were for the 131, 132, and 133 mass chains. The radiochemical 133 to 132 ratio of 1.02 ± 0.15 is in agreement with the mass spectrometric value of 1.155 ± 0.012. But the radiochemical 131 to 132 ratio of 0.54 ± 0.07 is not in agreement with the mass spectrometric value of 0.747 ± 0.003. However, earlier radiochemical measurements by Cunninghame (44) give a 131 to 132 ratio of 0.83 ± 0.10 which agrees with the mass spectrometric value.

DISCUSSION

COMPARISON WITH YIELDS FOR OTHER FISSIONABLE NUCLIDES

The fission cross-section of Am^{241} differs considerably from that of other fissionable nuclides whose yields have been measured with a mass spectrometer. It is much smaller and is characterized by relatively large resonances (51). The fission cross-section is shown in Figure 19 as a function of energy. Also shown in Figure 19 for comparison are the cross-sections of U^{235} (52), Pu^{239} (52), and Pu^{241} (53). Because the cross-section of Am^{241} is different, one might expect the fission-product yield pattern to be different also.

In actual fact, however, the yields are remarkably similar. The yields of the 131, 132, 133, 134, and 136 mass chains are shown in Figure 20 for U^{235}, Pu^{239}, U^{233}, Pu^{241}, and Am^{241}. It can be seen that the fine structure of the Am^{241} yield pattern is more pronounced than that of the U^{233} pattern but is less pronounced than that for Pu^{239} and much less than that for U^{235} and Pu^{241}.

There appears to be a correlation between the extent of fine structure and the neutron-proton ratio of the compound fissioning nucleus. As the neutron-proton ratio increases, the extent of fine structure increases. (See Table 13). On the basis of this correlation, one would predict the fine structure of the Am^{242} yield curve to be greater than that for Am^{241}. This was experimentally observed as can be seen from Figure 17. Here the 134 to 132 yield ratio is taken as a measure of the extent of fine structure. The 136 to 132 yield ratio is also greater for Am^{242}. This indicates that the slope of the low mass side of the heavy mass hump is greater for Am^{242} than for Am^{241}.

FIGURE 19 FISSION CROSS-SECTIONS

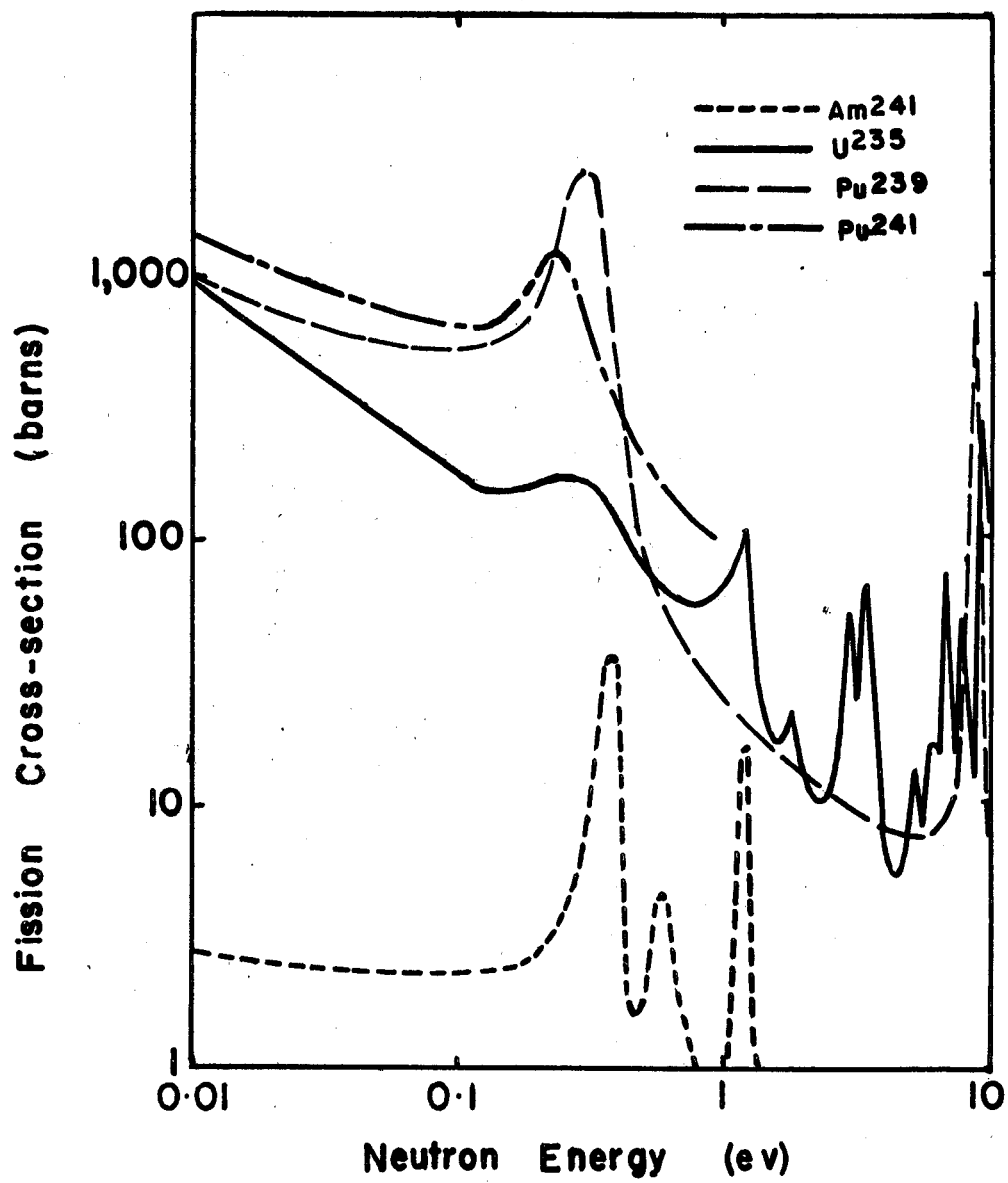

FIGURE 20 ABSOLUTE YIELDS IN THE XENON MASS REGION FOR VARIOUS FISSIONABLE NUCLIDES

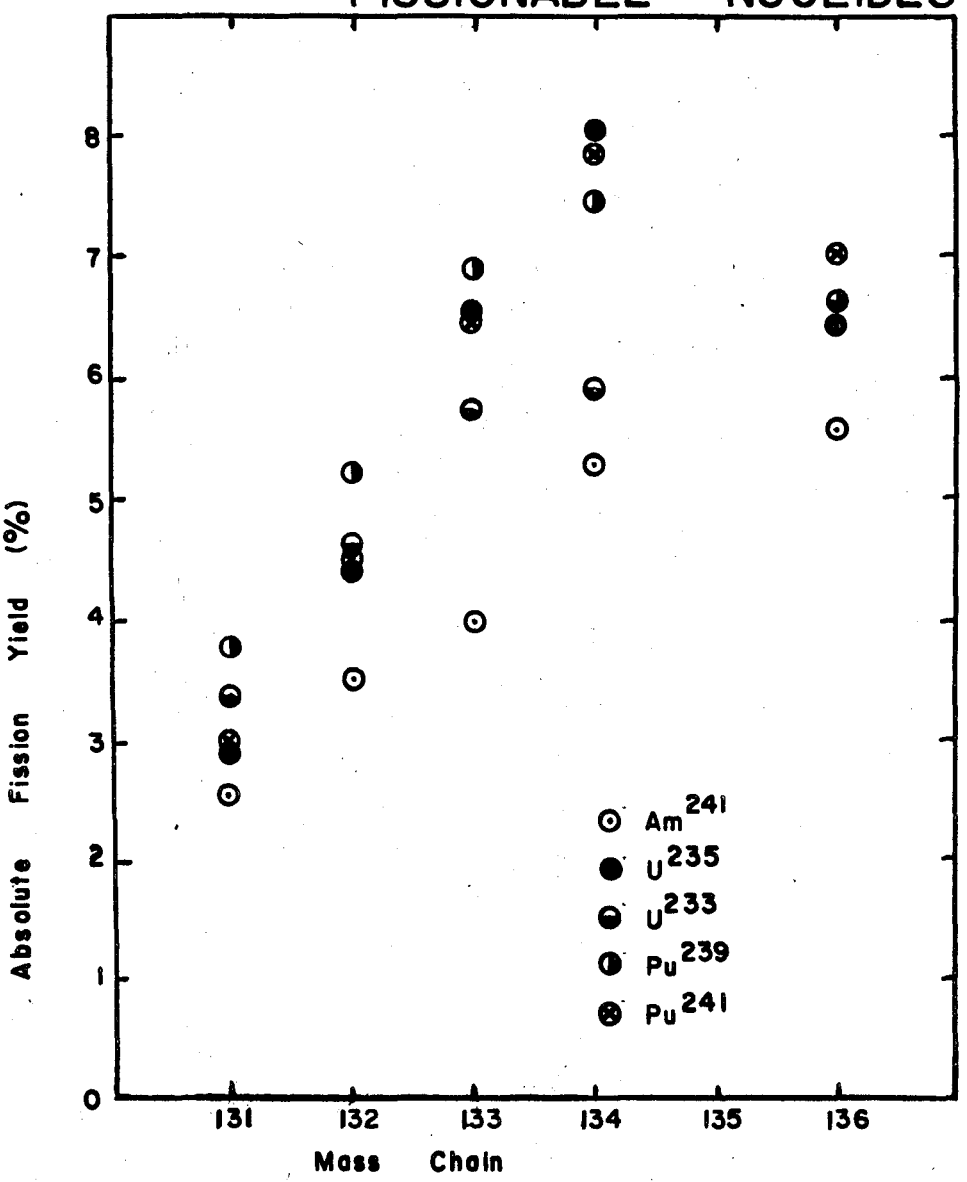

TABLE 13

Relationship between Extent of Fine Structure and Neutron-Proton Ratio of Compound Fissioning Nucleus

Fissioning Nuclide	Neutron-Proton Ratio of Compound Fissioning Nucleus	Extent of Fine Structure
U^{233}	1.543	slight
Am^{241}	1.547	moderate
Pu^{239}	1.553	moderate
U^{235}	1.565	large
Pu^{241}	1.574	large

RELATIONSHIP BETWEEN NEUTRON ENERGY AND FINE STRUCTURE

Changes in fine structure resulting from changes in the incident neutron energy have not been previously observed. An attempt to observe such an effect by comparing the fission yield pattern for cadmium-wrapped U^{235} using radiochemical methods did not reveal any measurable change (54). However, Croall and Willis (55) found a different ratio of the 77 mass chain yield to the 78 yield for cadmium-wrapped Pu^{239} as opposed to unwrapped Pu^{239}. The absolute yields of these mass chains are very low and they lie on the low mass tail of the light mass hump of the fission yield curve. Although this change in ratio does not in itself constitute a change in fine structure of the humps in the yield curve, it indicates that such an effect may exist. The mass spectrometer measurements of americium yields do reveal changes in fine structure.

Table 10 gives the yield data of the cadmium-wrapped sample of Am^{241}. The irradiation conditions were such that the number of Am^{242} fissions was negligible. It can be seen that the fine structure is significantly less than that for the unwrapped samples of Am^{241}. This means that neutrons of epithermal energy give a yield pattern for Am^{241} with less fine structure than neutrons of thermal energy. By comparing the capture cross-section of cadmium (see Figure 21) with the fission cross-section shown in Figure 19, it appears that the majority of fissions in the cadmium-wrapped sample was due to resonances in the fission cross-section at 0.58 ev and 1.25 ev. The large resonance at 0.30 ev was effectively shielded by the cadmium. An estimate of the total amount of xenon formed in the cadmium-wrapped sample as compared to the unwrapped samples was made using isotope dilution techniques. This estimate indicates that less than 10% of the number of fissions in the unwrapped samples was due to the resonances at 0.58 ev and 1.25 ev.

FIGURE 21 NEUTRON CAPTURE CROSS-SECTION OF CADMIUM

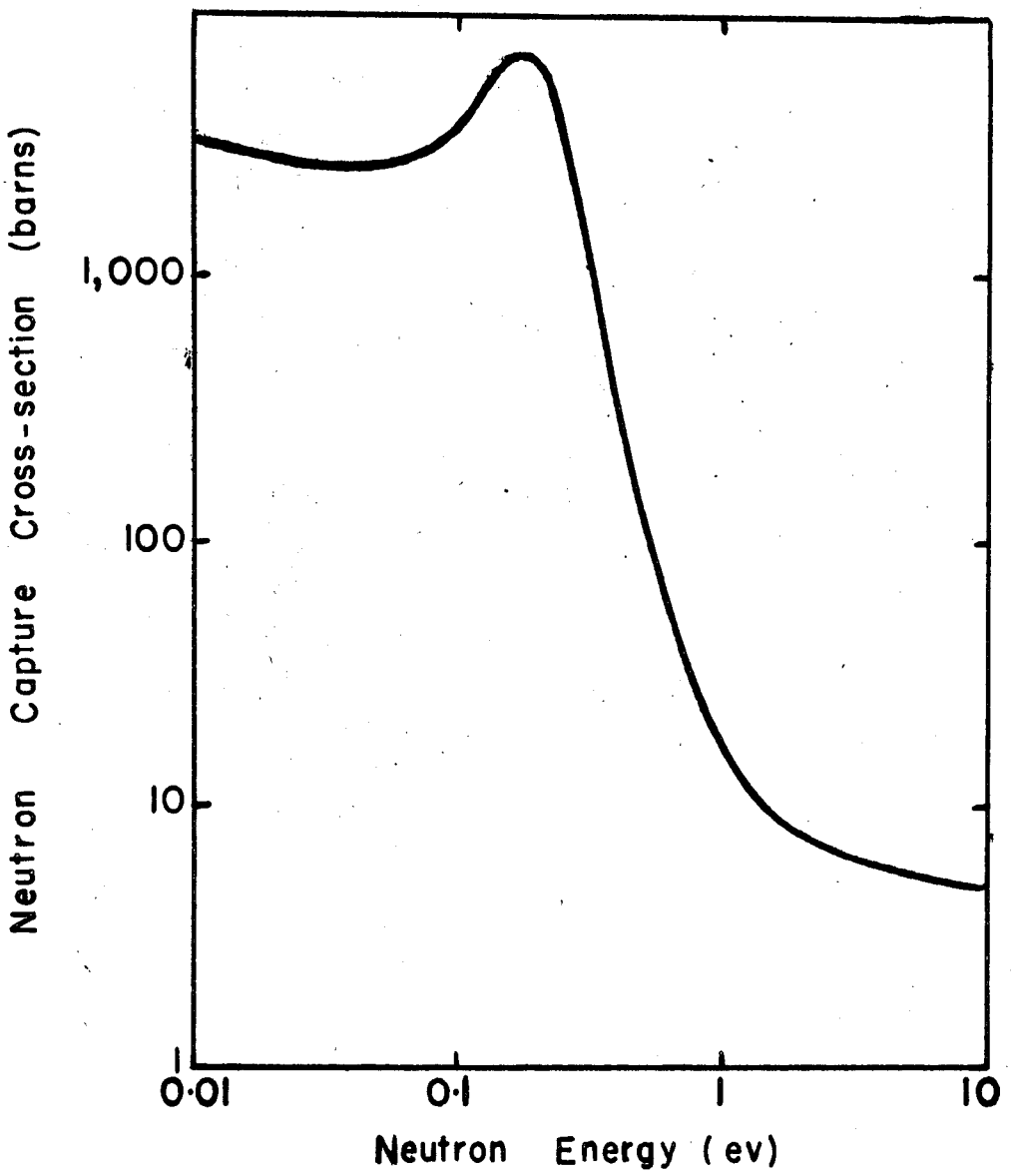

There is also evidence of an energy effect in the yield curve of Am^{242}. This can be seen by examining the curve in Figure 17 which shows how the 134 to 132 yield ratio changes as the number of fissions of Am^{242} and Am^{242m} increases relative to the total number of fissions (of Am^{241}, Am^{242}, and Am^{242m}). Points to the left of the curve correspond to short irradiation times and most of the fissions here are due to Am^{241}. Proceeding to the right along the curve (increasing irradiation time) there are two important changes. Not only is the number of fissions of 16.0 hour Am^{242} increasing relative to the number of Am^{241} fissions, but also the number of fissions of 152 year Am^{242m} is increasing relative to that of 16.0 hour Am^{242}. That this is so can be seen in Table 3. The curve in Figure 17 indicates that the fine structure increases as the number of fissions of 16.0 hour Am^{242} increases up to a point where the number of fissions of Am^{242m} becomes significant. Then it starts to drop. This indicates that the fine structure is less for Am^{242m} fission than for 16.0 hour Am^{242} fission.

The rest energy of 152 year Am^{242m} is 48.6 kev higher than that of 16.0 hour Am^{242} (56). Therefore, the compound nucleus, Am^{243}, formed by the capture of a thermal neutron by Am^{242m} will have 48.6 kev more excitation energy than a compound nucleus formed by the capture of a thermal neutron by Am^{242}. In fact, it will have the same excitation energy as a compound nucleus formed by the capture of a 48.6 kev neutron by Am^{242}. Let us assume that the compound nucleus remains intact long enough so that when it finally undergoes fission, all information about the state of the nucleus prior to neutron capture has been destroyed. This is a reasonable assumption, because, according to the liquid drop model, a U^{236} compound nucleus oscillates 10^7 times before undergoing fission. This would mean that the thermal neutron fission of Am^{242m} is equivalent to the 48.6 kev neutron fission of Am^{242}. Since the fine

structure appears to be less for the thermal neutron fission of Am^{242m} than for that of Am^{242}, it can be concluded that the fine structure for Am^{242} varies with neutron energy.

It is interesting that, in these experiments with Am^{241} and Am^{242}, the fine structure decreases as the neutron energy increases. It is known that the peak-to-valley ratio for fission yield curves tends to be greatest for spontaneous fission, less for resonance fission, still less for thermal neutron fission, and least for fast fission. This indicates that the fission process is most selective for spontaneous fission and least selective for fast fission. The variation in fine structure for Am^{242} is in accordance with this trend. On the other hand, one might have expected the fine structure to increase for the cadmium-wrapped sample of Am^{241} because of the resonances. However, the experiments with Am^{241} show that the fine structure decreases with increasing neutron energy whether or not resonances are involved.

Peak-to-valley ratio variations are usually explained in terms of the "two-mode theory of fission" (57) which states that the mass yield curve is the result of the superposition of a single-humped yield curve corresponding to a preference for symmetric fission and a double-humped curve corresponding to a preference for asymmetric fission. For low excitation energies of the compound nucleus, the asymmetric mode is predominant and this leads to a high peak-to-valley ratio. For high excitation energies (resulting from incident neutrons of high energy), the symmetric mode becomes more important and the peak-to-valley ratio is correspondingly lower. However, the two-mode theory does not predict a change in fine structure with increasing neutron energy. The observed changes are therefore an additional effect.

XENON-KRYPTON RATIO

The xenon-krypton ratios for the various samples are given in Table 9. These values, along with the normalized xenon yields given in Table 12, have been used to calculate the absolute krypton yields for Am^{241} as shown in Figure 22. It can be seen that the krypton yields give information about the low mass side of the light mass hump in the yield curve. In general, an increase in the mass number of the fissioning nuclide causes the light mass hump to move to the right. One might therefore expect that the xenon-krypton ratio for Am^{242} would be greater than that for Am^{241}. This is because the krypton yields are on the tail of the light mass hump and even a slight movement of the hump should have a large effect on absolute yields in that mass region. Yet the ratios in Table 9 indicate that they are roughly the same.

This can be explained by the Mathews-Tomlinson fission model as outlined in the INTRODUCTION. The width of the humps in the yield curve depends on the number of nucleons in the neck of the "dumb-bell". If the indentation at the 50-neutron shell were as great as at the 82-neutron-50-proton shell, then the yield patterns for two different fissioning nuclides would appear as in the top part of Figure 23. The low mass side of each hump would remain fixed while the heavy mass side of each hump would move to the right with an increase in mass of the fissioning nuclide. This means that the xenon-krypton ratio would be independent of the mass of the fissioning nuclide. (Actually, the ratio would be slightly affected by the neutron-proton ratio of the fissioning nucleus because the most probable mass of a fission fragment with 50 neutrons would be altered.) However, the indentation at the 50-neutron shell is less than at the 82-neutron-50-proton shell, according to Mathews-Tomlinson model, and therefore the yield patterns appear as in the bottom part of Figure 23. Nevertheless, the 50-neutron shell does

FIGURE 22 MASS YIELD CURVE OF Am^{241}

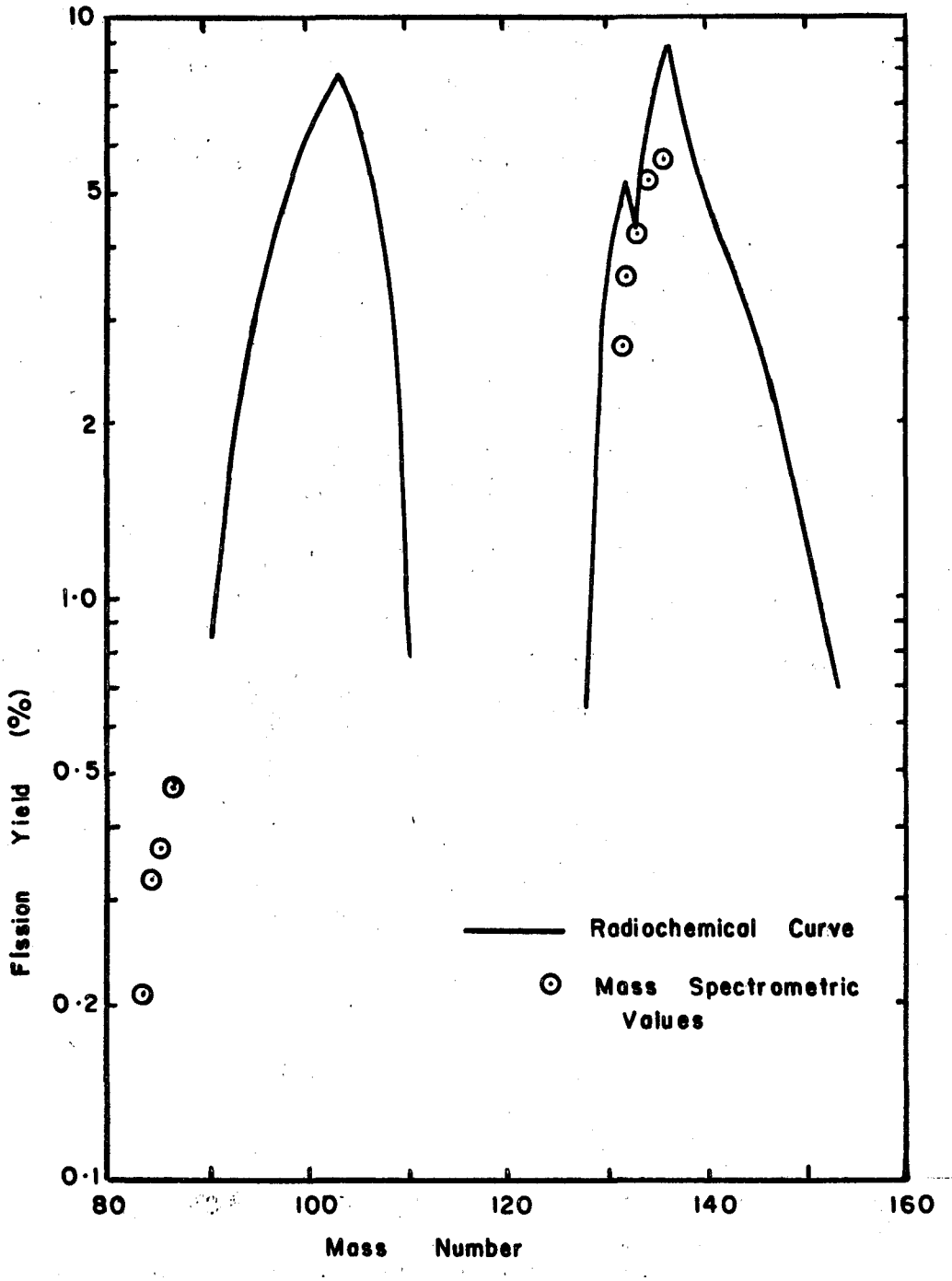

FIGURE 23 RELATIONSHIP BETWEEN POSSIBLE SHAPE OF FISSIONING NUCLEUS AND MASS YIELD CURVE

FOR EQUAL INDENTATIONS IN NECK NEXT TO CLOSED SHELLS:

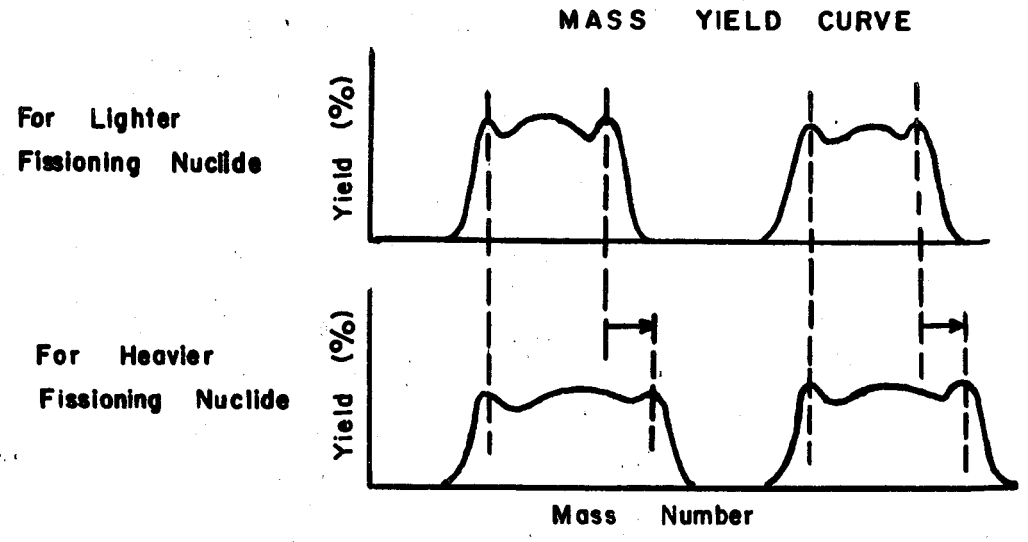

FOR UNEQUAL INDENTATIONS (MATHEWS-TOMLINSON MODEL):

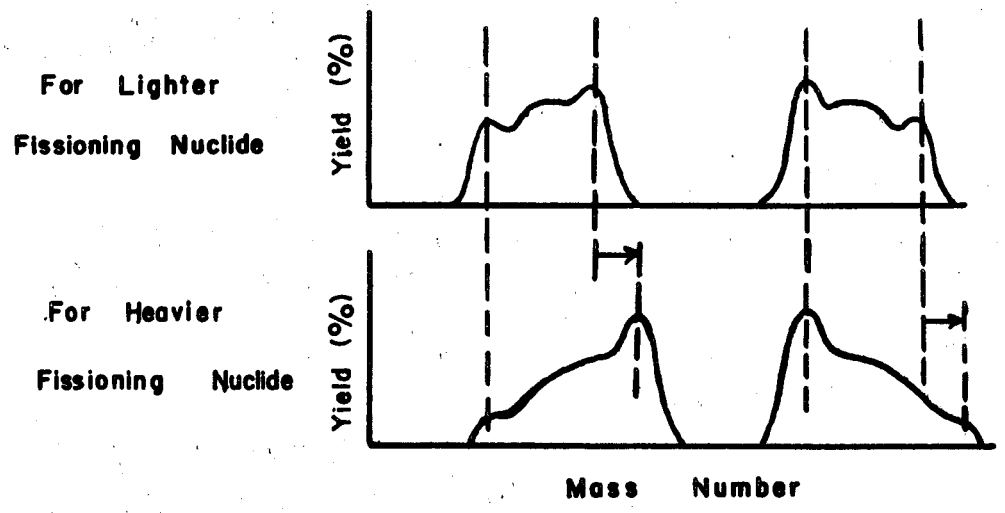

exert some influence and tends to prevent the low mass side of the light mass hump from moving to the right as the mass of the fissioning nuclide increases. The xenon-krypton ratio for U^{235} is about 5. If it were not for this holding effect of the 50-neutron shell, the ratio for both Am^{241} and Am^{242} would undoubtedly be much greater than the observed values of about 10.

KRYPTON YIELDS

The krypton yields by themselves do not seem to reveal any important features of the fission process. The pattern shows little change between Am^{241} and Am^{242}.

INDEPENDENT YIELD OF I^{130}

The independent yield of the shielded nuclide I^{130} gives information about the charge distribution curve for nuclear fission. The I^{130} yield measurements for Am^{241} given in Table 6 show that there is a marked change when the sample is irradiated with epithermal neutrons as opposed to thermal neutrons, i.e., the yield is twice as high. This indicates, for the first time, that neutrons of higher energy tend to spread out the charge distribution curve. This is further evidence that fission at higher excitation energies is a less selective process.

CONCLUSIONS

The mass spectrometric measurements of the fission yields of Am^{241} and Am^{242} have revealed a number of important features of the fission process.

(a) There is a direct relationship between the amount of fine structure at mass 134 and the neutron-proton ratio of the fissioning nucleus for thermal-neutron-induced fission.

(b) It has been shown for the first time that the fine structure in the mass yield curve decreases as the energy of the incident neutron increases.

(c) The 50-neutron shell in the fissioning nucleus has a significant effect on the shape of the mass yield curve.

(d) It has been shown for the first time that an increase in neutron energy changes the charge distribution in nuclear fission.

APPENDIX I

CORRECTIONS TO 136 MASS YIELDS

Some of the Xe^{136} in the samples is formed by neutron capture of fission-produced Xe^{135}. In order to obtain the true fission yield of Xe^{136}, it is necessary to subtract the amount of Xe^{136} formed by neutron capture of Xe^{135} from the measured amount of Xe^{136}. Also, the independent yield of Cs^{136} (45) must be added to the corrected Xe^{136} yield in order to obtain the yield of the entire 136 mass chain.

The longer-lived members at the end of the 135 mass chain are shown below.

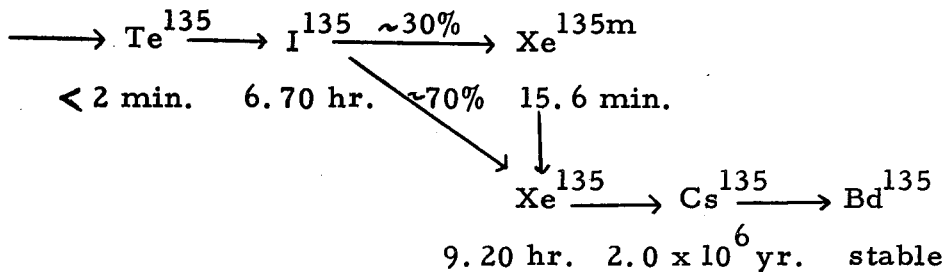

In order to simplify the calculations, one can reasonably assume that the independent yields of Xe^{135} and Cs^{135} are small enough to be neglected. Because of the very short half-lives of the precursors of I^{135}, it can then be assumed for purposes of calculation that all fission products of mass 135 initially appear as I^{135}. It can also be assumed that all of the I^{135} decays directly to the ground state of Xe^{135} instead of partially decaying through 15.6 min. Xe^{135m}. These last two assumptions lead to very little error because the shortest irradiation time (10 hours) is very long compared to the half-lives of Te^{135} and Xe^{135m}.

The differential equation which describes the number of I^{135} atoms which are present at any time during irradiation is

$$\frac{dN_1}{dt} = N_o Y_{135} \sigma_f \varphi - \lambda_1 N_1$$

where N_1 = number of atoms of I^{135}
N_o = number of fissionable atoms
Y_{135} = yield of 135 mass chain
σ_f = fission cross-section
φ = neutron flux
λ_1 = decay constant of I^{135}

Setting $N_1 = O$ when $t = O$ gives the following solution

$$N_1 = \frac{N_o Y_{135} \sigma_f \varphi}{\lambda_1} (1 - e^{-\lambda_1 t}) \quad . \quad . \quad . \quad 5$$

The differential equation which describes the number of Xe^{135} atoms present at any time during irradiation is

$$\frac{dN_2}{dt} = \lambda_1 N_1 - \lambda_2 N_2 - \varphi \sigma_c N_2$$

where N_2 = number of Xe^{135} atoms present
λ_2 = decay constant of Xe^{135}
σ_c = neutron capture cross-section of Xe^{135}

Setting $N_2 = O$ when $t = O$ and using equation 5 gives the following solution

$$N_2 = N_o Y_{135} \sigma_f \varphi \left[\frac{\left[1 - e^{-(\lambda_2 + \varphi \sigma_c)t} \right]}{(\lambda_2 + \varphi \sigma_c)} + \frac{\left[e^{-(\lambda_2 + \varphi \sigma_c)t} - e^{-\lambda_1 t} \right]}{(\lambda_2 + \varphi \sigma_c - \lambda_1)} \right] \quad . \quad 6$$

Let N_3 be the number of Xe^{136} atoms produced by the neutron capture of Xe^{135}

$$N_3 = \varphi \sigma_c \int_o^t N_2 \, dt$$

Using the expression for N_2 from equation 6 gives

$$N_3 = N_o Y_{135} \sigma_f \varphi^2 \sigma_c \left[\frac{t}{(\lambda_2 + \varphi \sigma_c)} - \frac{\left[1 - e^{-(\lambda_2 + \varphi \sigma_c) t}\right]}{(\lambda_2 + \varphi \sigma_c)^2} \right.$$

$$\left. + \frac{\left[1 - e^{-(\lambda_2 + \varphi \sigma_c) t}\right]}{(\lambda_2 + \varphi \sigma_c)(\lambda_2 + \varphi \sigma_c - \lambda_1)} - \frac{\left[1 - e^{-\lambda_1 t}\right]}{\lambda_1 (\lambda_2 + \varphi \sigma_c - \lambda_1)} \right] \quad . \quad . \quad . \quad 7$$

$$= N_o Y_{135} \sigma_f \varphi^2 \sigma_c \xi \quad . \quad . \quad . \quad 8$$

where ξ is the expression in the large square brackets in equation 7.

In the experiments, Xe^{136} was measured relative to Xe^{132}. Therefore, it is best to determine N_3 relative to the number of Xe^{132} atoms.

Let N_4 be the number of Xe^{132} atoms produced in fission.

$$N_4 = N_o Y_{132} \sigma_f \varphi$$

where Y_{132} = yield of 132 mass chain

$$\frac{N_3}{N_4} = \frac{Y_{135} \varphi \sigma_c}{Y_{132}} t \quad . \quad . \quad . \quad 9.$$

The true yield ratio of the 136 and 132 mass chains is given by

$$\frac{Y_{136}}{Y_{132}} = \left[\text{Measured ratio of } \frac{Xe^{136}}{Xe^{132}} \right] - \frac{N_3}{N_4} + \frac{C}{Y_{132}} \quad . \quad . \quad . \quad 10$$

where C = independent yield of Cs^{136}

It is necessary to know the values of $\frac{Y_{135}}{Y_{132}}$ and $\frac{C}{Y_{132}}$.

$$\frac{Y_{135}}{Y_{132}} = \left[\frac{Y_{135}}{Y_{133}}\right]\left[\frac{Y_{133}}{Y_{132}}\right] \quad \ldots \quad 11$$

$$\frac{C}{Y_{132}} = \left[\frac{C}{Y_{133}}\right]\left[\frac{Y_{133}}{Y_{132}}\right] \quad \ldots \quad 12$$

According to the radiochemical yield measurements made by Rickard et al. (45),

$$Y_{133} = 4.0 \pm 0.2\%$$

$$Y_{135} = 4.8 \pm 0.3\%$$

$$C = 0.16\%$$

Using these values along with the mass spectrometrically-measured value of 1.15 ± 0.02 for $\left[\frac{Y_{133}}{Y_{132}}\right]$ in equations 11, 12, and 9, equation 10 becomes

$$\frac{Y_{136}}{Y_{132}} = \left[\text{Measured ratio of } \frac{Xe^{136}}{Xe^{132}}\right] - \frac{1.38\,\Phi\,\sigma_c\,\xi}{t} + 0.046$$

APPENDIX II

RELATIVE NUMBER OF FISSIONS OF Am^{242} AND Am^{242m} WITH RESPECT TO Am^{241}

16.0 Hour Am^{242}

The differential equation which describes the number of 16.0 hour Am^{242} atoms which are present at any time during irradiation is

$$\frac{dN_b}{dt} = N_a \sigma_{c1} \varphi - N_b \lambda$$

where N_b = number of Am^{242} atoms

N_a = number of Am^{241}

σ_{c1} = neutron capture cross-section of Am^{241} leading to production of 16.0 hour Am^{242}

φ = neutron flux

λ = decay constant of Am^{242}

Setting $N_b = O$ when $t = O$ gives the following solution

$$N_b = \frac{N_a \sigma_{c1} \varphi}{\lambda} (1 - e^{-\lambda t}) \quad . \quad . \quad . \quad 13$$

Let N(242) be the number of fissions of Am^{242}

$$N(242) = \int_o^t N_b \sigma_{242f} \varphi \, dt$$

where σ_{242f} = fission cross-section of 16.0 hour Am^{242}.

Using equation 13 gives

$$N(242) = \frac{N_a \sigma_{c1} \sigma_{242f} \varphi^2}{\lambda} \left[t - \frac{1}{\lambda} (1 - e^{-\lambda t}) \right]$$

Let N(241) be the number of fissions of Am^{241}.

$$N(241) = N_a \sigma_{241f} \varphi t \quad . \quad . \quad . \quad 14$$

where σ_{241f} = fission cross-section of Am^{241}

$$\frac{N(242)}{N(241)} = \frac{\sigma_{c1} \sigma_{242f} \varphi}{\sigma_{241f} \lambda} \left[\frac{t - (1/\lambda)(1 - e^{-\lambda t})}{t} \right] \quad . \quad . \quad . \quad 3$$

152-Year Am^{242m}

The differential equation which describes the number of Am^{242m} atoms which are present at any time during the irradiation is

$$\frac{dN_c}{dt} = N_d \sigma_{c2} \varphi - N_c \sigma_{cf} \varphi \quad . \quad . \quad . \quad 15$$

where N_c = number of Am^{242m} atoms

σ_{c2} = neutron capture cross-section of Am^{241} leading to the production of Am^{242m}

σ_{cf} = the sum of the fission and neutron capture cross-sections of Am^{242m}.

It is unusual to take into account the depletion of the product nuclide (in this case Am^{242m}) due to its own fission and capturing of neutrons as has been done in equation 15. However, both the fission and neutron capture cross-sections of Am^{242m} are unusually large (6400 and 5500 barns respectively) so that, for the longer irradiation times, the depletion is significant. Failure to take this into account

would result in a 10% error in the calculated fission ratio (to be derived below) for the 1000 hour irradiation.

The solution of equation 15 (found by setting $N_c = O$ when $t = O$) is

$$N_c = \frac{N_a \sigma_{c2}}{\sigma_{cf}} (1 - e^{-\sigma_{cf} \varphi t}) \quad . \quad . \quad . \quad 16$$

Let N(242m) be the number of fissions of Am^{242m}.

$$N(242m) = \int_o^t N_c \sigma_{242*} \varphi \, dt \quad . \quad . \quad . \quad 17$$

where σ_{242*} = fission cross-section of Am^{242m}

Combining equations 14, 16, and 17 gives

$$\frac{N(242m)}{N(241)} = \frac{\sigma_{c2} \sigma_{242*f}}{\sigma_{cf} \sigma_{241f}} \left[1 - \frac{(1 - e^{-\varphi \sigma_{cf} t})}{\varphi \sigma_{cf} t} \right] \quad . \quad . \quad . \quad 4$$

BIBLIOGRAPHY

1. Hahn, O., and Strassmann, F., Naturwissenschaften 27, 11, 89 (1939).
2. Meitner, L., and Frisch, O.R., Nature 143, 239 (1939).
3. Bohr, N., and Wheeler, J.A., Phys. Rev. 56, 426 (1939).
4. Nier, A.O., Booth, E.T., Dunning, J.R., and Grosse, A.V., Phys. Rev. 57, 546, 748 (1940).
5. Steinberg, E.P., Freedman, M.S., National Nuclear Energy Series, Division IV, Vol. 9, Part V, McGraw-Hill, New York, Toronto and London (1951) p. 1378.
6. Thode, H.G., and Graham, R.L., Can. J. Res: A25, 1 (1947).
7. Macnamara, J., Collins, C.B., and Thode, H.G., Phys. Rev. 78, 129 (1950).
8. Petruska, J.A., Thode, H.G., and Tomlinson, R.H., Can. J. Phys. 33, 693 (1955).
9. Farrar, H., and Tomlinson, R.H., Nucl. Phys. 34, 367 (1962).
10. Farrar, H., Fickel, H.R., and Tomlinson, R.H., Can. J. Phys, 40, 1017 (1962).
11. Fleming, W.H., and Thode, H.G., Can. J. Chem. 34, 193 (1956).
12. Farrar, H., Clarke, W.B., Thode, H.G., and Tomlinson, R.H., Can. J. Phys. 42, 2063 (1964).
13. Young, B.G., and Thode, H.G., Can. J. Phys. 38, 1 (1960).
14. Wanless, R.K., and Thode, H.G., Can. J. Phys. 33, 541 (1953).
15. Harvey, J.W., Clarke, W.B., Thode, H.G., and Tomlinson, R.H., Can. J. Phys. 44, 1011 (1966).
16. Fleming, W.H., Tomlinson, R.H., and Thode, H.G., Can. J. Phys. 32, 522 (1954).

17. Steinberg, E. P., and Glendenin, L. E., Phys. Rev. 95, 431 (1954).

18. Nervik, W. E., Phys. Rev. 119, 1685 (1960).

19. Laidler, J. B., and Brown, F., J. Inorg. and Nucl. Chem. 24, 1485 (1962).

20. Wiles, D. R. and Coryell, C. D., Phys. Rev. 96, 696 (1954).

21. Duffield, R. B., Schmitt, R. A., and Sharp, R. A., Proceedings of the Second United Nations Conference on the Peaceful Uses of Atomic Energy, Vol. 15, United Nations, Geneva (1958) p. 202.

22. Meason, J. L., and Kuroda, P. K., Phys. Rev. 142, 691 (1966).

23. Glendenin, L. E., Phys. Rev. 75, 337 (1949).

24. Pappas, A. C., Laboratory for Nuclear Science, M. I. T., Technical Report No. 63 (1953).

25. Glendenin, L. E., Steinberg, E. P., Ingram, M. G., and Hess, D. C., Phys. Rev. 84, 860 (1951).

26. Wiles, D. R., Smith, B. W., Horsley, R., and Thode, H. G., Can. J. Phys. 31, 419 (1953).

27. Farrar, H., and Tomlinson, R. H., Can. J. Phys. 40, 943 (1962).

28. Whetstone, S. L. Jr., Phys. Rev. 114, 581 (1959).

29. Apalin, V. F., Dobrinin, Y. P., Zakharova, V. P., Kutikov, I. E., and Mikaelyan, L. A., Soviet J. Atomic Energy 8, 10 (1961).

30. Milton, J. C. D., and Fraser, J. S., Can. J. Phys. 40, 1626 (1962).

31. Wahl, A. C., Ferguson, R. L., Nethaway, D. R., Troutner, D. E., and Wolfsberg, K., Phys. Rev. 116, 382 (1959).

32. Glendenin, L. E., Coryell, C. D., and Edwards, R. R., in "Radiochemical Studies: The Fission Products, Book 1", edited by Coryell, C. D., and Sugarman, N.; National Nuclear Energy Series, McGraw-Hill, New York, (1951) p. 489.

33. Pappas, A. C., Proceedings of the United Nations Conference on the Peaceful Uses of Atomic Energy, Vol. 7, United Nations Geneva (1955) p. 19.

34. Kennett, T. J., and Thode, H. G., Phys. Rev. 103, 323 (1956).

35. Fong, P., Phys. Rev. 102, 434 (1956).

36. Stein, W. E., and Whetstone, S. L. Jr., Phys. Rev. 110, 476 (1958).

37. Brunner, W., and Paul, H., Ann. der Phys. 7. Folge 6, 267 (1960).

38. AERE-TRANS-897 U. K. A. E. A. Report, Sykes, J. B. (1962).

39. Harvey, J. W., Ph. D. Thesis, McMaster University (1965).

40. Fraser, J. S., and Milton, J. C. D., Phys. Rev. 93, 818 (1954).

41. Mathews, C. K., Ph. D. Thesis, McMaster University (1964).

42. Seaborg, G. T., James, R. A., and Morgan, L. O. in "The Transuranium Elements" edited by Seaborg, G. T., Katz, J. J., and Manning, W. M.; National Nuclear Energy Series, McGraw-Hill, New York, (1949) p. 1525.

43. Ghiorso, A., James, R. A., Morgan, L. O., and Seaborg, G. T., Phys. Rev. 78, 472 (1950).

44. Cunninghame, J. G., J. Inorg. Nucl. Chem. 4, 1 (1957).

45. Rickard, R. R., and Goeking, C. F., and Wyatt, E. I., Nucl. Sci. Eng. 23, 115 (1965).

46. Katz, J. L., and Seaborg, G. T., "The Chemistry of the Actinide Elements", Methuen, London (1957) p. 358.

47. Tomlinson, R. H., McMaster University, Private Communication.

48. Kennett, T. J., Ph. D. Thesis, McMaster University (1956).

49. Clarke, W. B., and Thode, H. G., Can. J. Phys. 42, 213 (1964).

50. Sullivan, W. H., "Trilinear Chart of Nuclides", U. S. Government Printing Office, Washington.

51. HW-56919 Nuclear Physics Quarterly Report for April, May, and June, 1958. General Electric Co. Hanford Atomic Products Operation, Richland, Wash.

52. Hyde, E. K., "The Nuclear Properties of the Heavy Elements, Vol. III - Fission Phenomena", Prentice Hall, Englewood Cliffs, N. J. (1964) p. 60.

53. HW-58000 Plutonium Recycle Program. Annual Report, Fiscal Year, 1958. S. Goldsmith. '58.

54. Los Alamos Radiochemistry Group, Phys. Rev. 107, 325 (1957).

55. Croall, I. F., and Willis H. H., Proceedings of the Salzburg Symposium on Physics and Chemistry of Nuclear Fission, Vol. I, International Atomic Energy Agency, Vienna (1965) p. 355.

56. Asaro, F., Perlman, I., Rasmussen, J. O., and Thompson, S. G., Phys. Rev. 120, 934 (1960).

57. Turkevich, A., and Niday, J. B., Phys. Rev. 84, 52 (1951).